Theses and Dissertations

May 2016

3D SEM Surface Reconstruction: An Optimized, Adaptive, and Intelligent Approach

Ahmad Pahlavan Tafti
University of Wisconsin-Milwaukee

Follow this and additional works at: https://dc.uwm.edu/etd

Part of the Artificial Intelligence and Robotics Commons

3D SEM Surface Reconstruction: An Optimized, Adaptive, and Intelligent Approach

by

Ahmad Pahlavan Tafti

A Dissertation Submitted in

Partial Fulfillment of the

Requirements for the Degree of

Doctor of Philosophy

in Engineering

at

The University of Wisconsin–Milwaukee

May 2016

ABSTRACT

3D SEM Surface Reconstruction: An Optimized, Adaptive,
and Intelligent Approach

by

Ahmad Pahlavan Tafti

The University of Wisconsin–Milwaukee, 2016
Under the Supervision of Professor Zeyun Yu

Structural analysis of microscopic objects is a longstanding topic in several scientific disciplines, including biological, mechanical, and material sciences. The scanning electron microscope (SEM), as a promising imaging equipment has been around to determine the surface properties (e.g., compositions or geometries) of specimens by achieving increased magnification, contrast, and resolution greater than one nanometer. Whereas SEM micrographs still remain two-dimensional (2D), many research and educational questions truly require knowledge and information about their three-dimensional (3D) surface structures. Having 3D surfaces from SEM images would provide true anatomic shapes of micro samples which would allow for quantitative measurements and informative visualization of the systems being investigated. In this research project, we novel design and develop an optimized, adaptive, and intelligent multi-view approach named 3DSEM++ for 3D surface reconstruction of SEM images, making a 3D SEM dataset publicly and freely available to the research community. The work is expected to stimulate more interest and draw attention from the computer vision and multimedia communities to the fast-growing SEM application area.

TABLE OF CONTENTS

LIST OF FIGURES

vii

LIST OF TABLES

ACKNOWLEDGEMENTS

First, I would like to express my sincere gratitude to my advisor Prof. Zeyun Yu for the continuous support of my Ph.D study and research, for his patience, motivation, and immense knowledge. His insightful thoughts and advice helped me in all the time of research and writing of this thesis.

Besides my advisor, I would very much like to thank all my thesis committee members: Prof. Ethan Munson, Prof. Ichiro Suzuki, Prof. Ramin Pashaie, and Dr. Heather A. Owen, for their valuable comments and encouragement.

My sincere thanks also go to Andrew B. Kirkpatrick and Jessica D. Holz, who provided me an opportunity to join them in the Biological Sciences Electron Microscopy Lab at UW-Milwaukee, and who gave access to the SEM micrographs and research facilities. Without their precious support it would not be possible to conduct this research.

Last but not the least, I would like to thank my bountiful family: my wife, Elham, and my daughter, Sara, for supporting me spiritually throughout writing my PhD thesis and in my life in general.

Chapter 1

Introduction

1.1   Background and Problem Statement

3D surface reconstruction from a set of 2D images has been a very active research area in computer vision and artificial intelligent over the past decades and has led to a broad range of real-world applications including 3D world scene reconstruction, movie making, medical visualization, virtual tourism, mobile robot navigation, virtual reality, and computer aided design [7], [33], [54], [74], [77], [101], [105], [125].

The technique of Scanning Electron Microscope (SEM) imaging has also been traditionally employed in a variety of research areas to "view" the surface structure of microscopic samples [18], [19], [24], [26], [43], [89], [96]. However, SEM images still remain two-dimensional (2D). Having truly three-dimensional (3D) shapes from SEM micrographs would provide anatomic surfaces allowing for quantitative measurements and informative visualization of the objects being investigated. Many facets of science could benefit from 3D SEM surface reconstruction techniques. For instance, biological researchers can get 3D surface models of specimens to investigate their surface characteristics, such as recognizing roughness, flatness, and waviness. Medical researchers are interested in 3D modeling to inspect cell anatomy, taking advantages of virtual reality applications in medicine [96]. There are also many aims for material science and mechanical engineering in which 3D representation of material properties is critical to accurately measure a fractal dimension and surface roughness, designing a micro article which needs to fit into a tiny appliance [27], [29], [101], [94].

While in computer science rich work is available on algorithm designing and software developing of 3D surface reconstruction from 2D images [7], [33], [94], [125], little attention has been paid to adapting and optimizing these techniques for 3D SEM reconstruction.

Particularly, very few software tools are currently available. The one that has been commercialized is MeX [3], which is, however, very costly for small research groups with limited funding. Also, the installation and use of this software can be difficult for people without much IT experience.

For these reasons, the current research project will be focused on novel designing and developing an optimized, adaptive, and intelligent multi-view framework for 3D surface reconstruction of SEM images, making a 3D SEM dataset publicly and freely available to the research community. The present work is expected to stimulate more interest and open the doors from the computer vision community to the SEM and its application area.

1.2   The Scanning Electron Microscope

In electron microscopy, the source of illumination of the specimen comes from a beam of electrons [26]. The beam is generated in a vacuum by an object called an "electron gun". The basic construction of the electron gun comprises three key elements; a filament, a shield, and an anode. The filament serves as the source of electrons for the beam. Filaments can vary in composition from tungsten to lanthanum hexaboride [89]. The second component is the shield. The shield, also referred to as Wehnelt cylinder, bias shield, focusing electrode and grip cap, primarily functions to direct the emitted electrons in a downward trajectory in the column of the microscope. The final component is the anode. The disc like structure is located directly underneath the shield and aids in drawing electrons down into the column at a constant speed [18]. The electrons emitted from the gun are controlled by several electromagnetic lenses placed at various points within the column of the microscope. These lenses control the coherency of the beam, correct for spherical aberration and regulate spot size. In addition, SEMs exhibit an extra pair of coils called deflection coils, located near the final lens of the column. During the scanning operation, voltage passing through the coils is oscillated. This produces a magnetic field which influences the electron beam, causing it to move back and forth, or raster, across the specimen [26].

Table 1.1: Comparison of the SE and BSE imaging in a SEM

SE-based imaging	BSE-based imaging
Higher resolution and darker intensities	Lower resolution and brighter intensities
Inelastic scattering (low energy electrons)	Elastic scattering (high energy electrons)
Contains topographical information	Contains compositional information

As the beam is rastered, the electrons from the beam will interact with those residing at the surface of the sample. The interaction will subsequently yield two types of signal. One form of signal involves the electrons from the beam that collide with the sample and change trajectory without losing significant energy or momentum. These electrons are called elastically Backscattered Electrons (BSE). The detection of BSE signal has proven beneficial to compositional studies of unknown and synthesized materials. Commonly, the greater the atomic number of the element within a sample, the greater likelihood of generating BSE [26]. This relationship can be used to provide compositional information of a sample as elements with a greater atomic number will produce more BSE and a greater signal [89]. However, due to the high energy with which these electrons interact with the sample, it is possible for these electrons to conduct multiple collisions before escaping, as well as penetrate into the interior of the sample. These particular outcomes result in an excess of signal which negatively influences surface imaging through a reduction of resolution [26]. The other product is referred to as Secondary Electrons (SE). SE result from an inelastic collision between electrons of the beam and the sample. This transfer of energy can cause the sample to eject electrons of significantly lower energy levels than BSE or those comprising the beam [43], [89]. Due to the weak nature of the SE, only those produced at or near the surface are capable of escaping from the sample and producing a detectable signal [18], [19], [26]. It is for this reason that SE images have a higher resolution and greater topological contrast than images produced from BSE as seen in Figure 1.1. We have also summarized the main differences between SE and BSE based SEM imaging in Table 1.1.

3
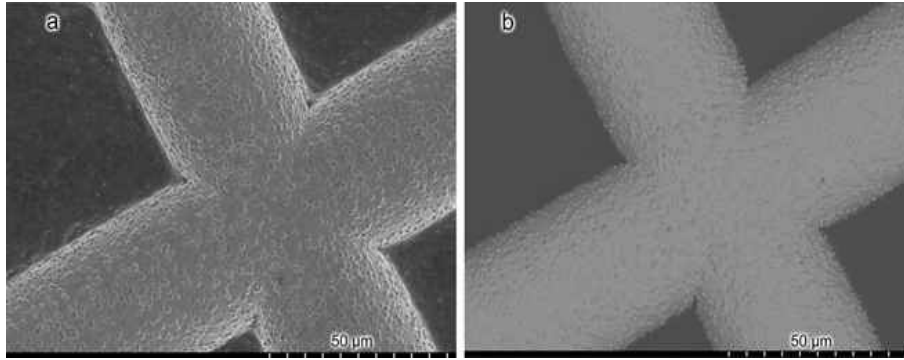
Figure 1.1: Secondary Electron (SE) and Backscattered Electron (BSE) micrographs of the same area of a TEM copper grid. SE micrograph (a) exhibits greater resolution and topography on the surface of the grid as well as of the background. It also provides darker intensities compared with BSE images. BSE micrograph (b) exhibits greater contrast and brightness between materials comprising the sample. Resolution compared to SE micrograph is much reduced.

1.3   3D Surface Reconstruction

3D surface reconstruction techniques constitute an important part of 3D computer vision and its subject matter [33], [73]. It compromises the construction of integrated vision systems to realistic problems existing in the real world. 3D surface reconstruction has often been used in the process of creating 3D shape models from only a set of 2D images [33], [54]. 3D Computer vision has provided an excellent ability to restore the 3D geometry information of a real scene by solving the inversion problem going from 2D to 3D. We list popular applications of 3D surface reconstruction in two categories as shown in Table 1.2 [7], [29], [33], [54], [73], [74], [77], [96], [101], [125].

The origin of 3D computer vision dates back to 1957 when Gilbert Hobrough illustrated a method and designed an apparatus for analog implementation of stereo image correlation [60]. In 1963, Larry Roberts proposed the first 3D surface reconstruction technique by developing a machine perception algorithm which could create and display 3D geometry information of objects from a single 2D photo [97]. Then, in 1970, B. P. Horn designed another 3D surface reconstruction technique called Shape-from-Shading (SFS) [61]. SFS used shading from an individual image in order to calculate the surface orientation. R. J. Woodham, in 1977, designed the Photometric Stereo (PS) algorithm [126] as a multi-view version of Shape-from-Shading . In 1990, C. Tomasi and T. Kanade were

4

Table 1.2: The popular applications of 3D surface reconstruction in industry, medicine, and entertainment.

Biomedical and Medical	Industrial and Commercial
3D Microscopy Vision	3D Representation of Mechanical Models
3D Modeling of Tissues	3D Representation of Material Properties
3D Tracking of Human Body Parts	Measurement of Fractal Dimension
Inspection of Surfaces	Pose Refinement, and Height Evaluation
Medical Visualization	CAD/CAM, Game, and Animation
Remote Surgery	Roughness Measurement
3D Modeling of Cells	Mobile Robot Navigation
Biomedicine and Medicine Virtual Reality	Virtual City and Virtual Museum

able to estimate 3D surface structure from a sequence of 2D images [116]. They proposed a method called Structure from Motion (SFM). In 2002, T. Zickler, P. N. Belhumeur, and D. Kriegman designed Helmholtz stereopsis [133] to reconstruct the 3D geometry of an object from a collection of 2D images. In 2011, J. Shotton et al. [103] provided a new method to predict 3D positions of body joints from a single depth image in a fast and accurate manner by recording the shape of the reflected points of light by means of a camera. Instead of temporal information, this was known as structured light (or light coding) capture. This technique has famously been used in Microsoft's Kinect accessory. Readers interested in 3D computer vision and 3D surface reconstruction are referred to [33], [54], [125] for further information.

1.4   3D Surface Reconstruction from SEM Images

The process of creating a 3D shape model of a microscopic sample is still rather difficult to solve since its three dimensional shape in the real world is only projected into and available as 2D digital images. Over the past few years, there has been an expansion in designing and developing 3D surface reconstruction algorithms for images obtained by a SEM. These algorithms can be categorized into three main classes: (1) Single-View [11], [23], [42], [62], [75], [88], [91], [104], (2) Multi-View [94], [101], [114], [134], and (3) Hybrid [34].
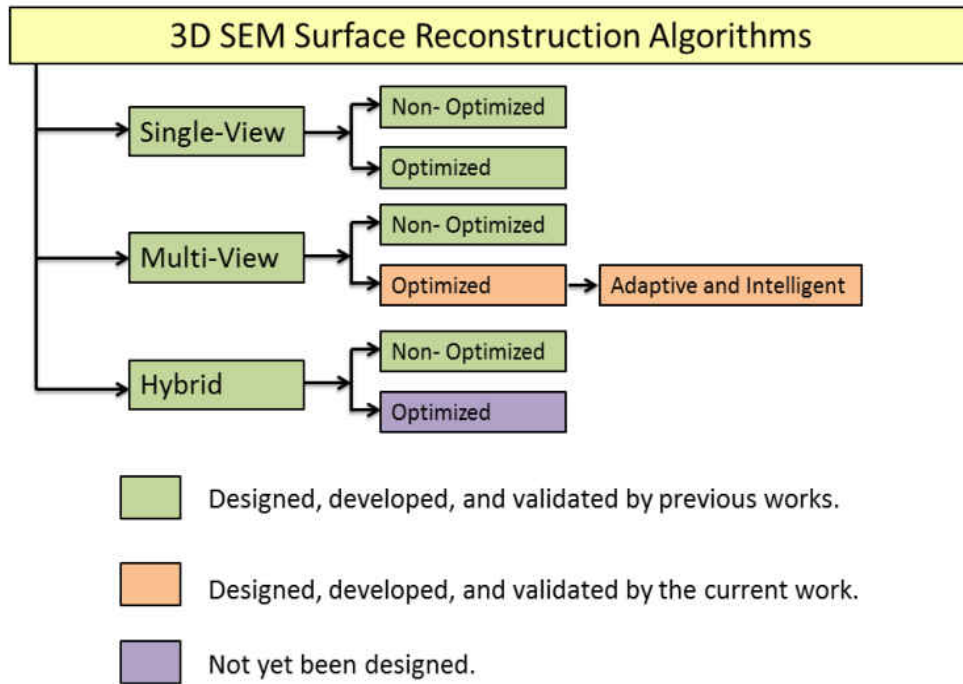
Figure 1.2: Taxonomy of 3D SEM surface reconstruction studies.

There have also been some sorts of 3D SEM volume reconstruction including Focused Ion Beam Scanning Electron Microscopy (FIB-SEM) and Electron Tomography (ET) [50], [67] in which they have tried to characterize the complex microstructure of a sample in the context of the whole. Using FIB-SEM or ET, a 3D volume of the object or sample is obtained through the acquisition and manipulation of a series of 2D projections [50]. The series of images are obtained over a range of directions and orientations. The point is that sample sectioning and possible destruction is required by these techniques but not in the 3D SEM surface reconstruction. In the current work, we only explore the use of 3D surface reconstruction techniques for SEM images, and not 3D volume reconstruction.

Figure 1.2 shows a taxonomy of 3D SEM surface reconstruction studies and highlights our scope in this contribution.

In the following, we reflect the current knowledge and progress in 3D SEM reconstruction of surfaces from 2D images.

6

1.4.1   Single-View Approach

In the Single-View approach, a set of 2D images from a single view point with varying light directions are considered for 3D SEM surface reconstruction. Photometric Stereo (PS) is the main algorithm used in this class to produce 3D geometry information of a microscopic sample [126]. PS is a 3D computer vision algorithm which rapidly computes the three dimensional geometry of an object by examining 2D images being viewed from the same viewpoint, but being illuminated from different directions. The PS method has five general steps: 1) Take a set of single view digital images of an object (sample) under the different light directions, 2) Determine the light directions, 3) Calculate surface normals, 4) Calculate Albedo (reflection coefficient), and 5) Depth estimation [58], [126]. Fundamental basics on the PS algorithm can be found in [76], [123].

For application of the PS method to scanning electron microscopy, several methods of implementation and instrumentation have been developed and utilized to improve the algorithm and make it more applicable to different areas of research. In 2005, Paluszynski et al. [88] developed a method of PS by applying signal processing methods and shape from shading to reconstruct the third dimension of smooth objects. This method assumes that the SE and BSE detectors distributed are based on the Lamberts Law distribution [123]. Since some instruments use only 2 detectors, this algorithm is not useful for them. In 2006, Drzazga et al. [42] developed a method of 3D surface reconstructions of SEM images. This method employed signal processing to eliminate the errors (i.e. distortions) such that the inspection of geometric issues in the micro structures is more feasible.

In 2006, Pintus et al. [91] proposed and tested a method for automatic alignment of PS performed via a BSE detector. This was proposed since PS is beneficial when sequential acquisition of the backscattered images is performed. This alignment in a SEM was completely controlled by computer, and the authors demonstrated the pixel precision of the reconstructed surface by using the PS method. In 2008, Argyriou et al. [11] developed an iterative PS algorithm in case of having multiple highlights and shadows. This algorithm was designed to work with at least 3 different light sources, and was capable of recognizing unreliable sources based on unreliable pixel intensities. While

most of the work has focused on 3D SEM surface reconstruction algorithms, less research effort has been spent on the effects of SEM variables and measurement parameters on 3D reconstruction accuracy. In 2008 Marinello et al. [80] investigated how SEM instrumental parameters influence the quality of 3D surface reconstruction, recognizing two main classes of various instrument and measuring factors. Their evaluations involved the operation of the most famous commercial software package for SEM surface reconstruction, namely Alicona MeX [3]. They found that image quality and its spatial resolution, magnification, relative position of detectors and tilt angle are among the most important parameters which affect the accuracy of 3D SEM surface reconstruction.

In 2013, Slowko et al. [104] carried out 3D surface reconstruction for images obtained by a SEM. This method was different in equipment, since it provided the environmental condition of vacuum where a vacuum-detector contained an intermediate vacuum chamber inside which there was a semiconductor BSE detector.

There are also some optimized versions of Single-View methods that use a refinement process in which both SEM parameters and 3D geometry information are optimized simultaneously. In 2005, Kodama et al. [69] used a genetic algorithm to solve the optimization problem employed in surface reconstruction of 2D images obtained from SE and BSE detectors in SEM systems. The Delaunay triangulation [87] was used for the coding. Since employing a genetic algorithm was computationally expensive, hybrid algorithms were used taking advantage of genetic algorithm and simulated annealing algorithm [66].

In 2007, Yuniarti et al. [130] solved the PS problem for the case of noisy images as inputs to the surface reconstruction algorithm. The noisy images make the problem require nonlinear optimization tools. To solve the nonlinear optimization problem, a 2D leap frog algorithm [71], [72] was employed, which converts one large problem into a number of smaller optimization problems. In this work, the effect of changing the size of the snapshots on the reconstruction algorithm was analyzed. Yuniarti et al. concluded that the larger snapshots improved the quality of the reconstructions, although the computation time would increase. Also, median filters were applied to the recovered surface to decrease the number of outliers. In 2010, Vynnyk et al. [121] implemented the PS tech-

nique focusing on the detector efficiency and the distribution of the electron beams based on the Cosine Lambert's Law [123]. The Cosine Lambert's Law is one of the requirements of the PS technique which was suppressed in this approach. As a result of employing this method, a high lateral and vertical resolution was obtained when measuring the structures. One of the main disadvantages of this method is that it is only capable of measuring samples with slope of up to 45 degrees; for larger angles the setup needs to be improved by optimizing the field distribution to which the sample is subjected. Vynnyk et al. used an atomic force microscope for the measurements as well as an SEM. Unlike other microscopes, this microscope does not damage the surface which makes it suitable for measuring topography data. The PS algorithm has found its application as a new tool in the semiconductor industry. One of these applications is monitoring the manufacturing process precisely to increase the quality of printed circuits. In 2013, Estellers et al. [45] used the PS method to implement the 3D surface reconstruction of images of printed circuits taken with SEM. This was done to compare the circuit details with the expected circuit which led also to a deformation field. This enabled the development of an optimization based surface reconstruction algorithm. The results showed robustness to noise and could be applied in the chip manufacturing industry to improve the precision of the lithographic process.

1.4.2 Multi-View Approach

In the Multi-View approach, a 3D computer vision algorithm is employed, namely Structure from Motion (SFM) [54], [116]. This method utilizes stereo pairs taken by tilting the micro object between photographs. SFM is established on the theory of projective geometry, with considering different perspectives from different view angles to restore the 3D structure of a specific object [54]. By using corresponding feature points in image pairs, a 3D point can be reconstructed by triangulation [54]. Basic requirements are the determination of camera calibration (intrinsic camera parameters) and pose (camera rotation and translation), which may be given by a 3×4 camera projection matrix. The projective geometry method allows the projection matrix and 3D points to be estimated

using only corresponding points in different views. The SFM method has five major steps [54], [116], [125]: 1) Take a set of digital images of an object (sample), 2) Identify key points in the images that can possibly be detected in other images in the set, 3) Search for corresponding points in images (this step is also called point-matching), 4) Use the projection geometry theory to estimate camera projection matrices, and 5) Compute 3D surface model using linear triangulation. Further details for the SFM algorithm can be found in [54].

In 2005, Raspanti et al. [94] presented a high resolution 3D reconstruction method based on the SFM algorithm. They firstly read a stereo pair of SEM images, then selected on the first picture a user defined number of prominent feature points. They also used Delaunay triangulation [87] to restore the spatial model of a micro sample. In 2007, Samak et al. [101] used a SFM algorithm to reconstruct 3D microstructure surfaces from SEM images. The proposed method first computed 3D points from 2D matched key points, then triangulated the 3D points into the 3D mesh, and finally mapped a 2D image as a texture on the shape model.

In 2011, Carli et al. [23] performed a theoretical uncertainty evaluation of stereo-pairs technique for 3D SEM surface reconstruction. Their work discussed 3D SEM surface reconstruction based on the Piazzesi model function applied to both stereo-pairs and multi-pairs matched through a rank-area-based method. Uncertainty tables have been presented for the different cases of tilt and rotation in a SEM. Pixel size and rotation angle are areas with the greatest degree of uncertainty in 3D SEM stereo-pairs surface reconstruction. In 2013, Zolotukhin et al. [134] examined the advantages and limitations of the Structure from Motion approach to perform 3D reconstruction for SEM images. It was concluded that the algorithm is applicable to build a 3D model of a micro object. Their proposed traditional SFM algorithm received two images from two camera angles, found the correspondence key points, estimated the mutual positions of the images using the RANSAC algorithm [47], [54], and built a 3D surface. They did not mention that we may have some invaluable information about SEM camera calibration which is useful to increase the accuracy of the algorithm and reduce the processing time. For example, we

have all intrinsic parameters of a SEM, including focal length, principal point coordinate and horizontal and vertical resolution.

1.4.3 Hybrid Approach

The third class of 3D SEM surface reconstruction algorithms is called the Hybrid method, and it offers a compromise between the Single-View and the Multi-View approaches. In 2003, Danzl et al. [34] presented an algorithm to reconstruct surfaces and 3D images by applying stereo and shading information from two 2D images. The stereo and shading information are complementary requirements of the reconstruction, since shape from shading does the reconstruction very well when the 2D data has homogeneous texture and shape from stereo helps when there are various features in the data. Despite previous works which assumed the reflectance map to be known or given by simple mathematical functions, their work estimated the reflectance map by using a fitting polynomial of degree 4 and used the stereo and shading information simultaneously. The latter was an optimization problem where it minimized an energy function with constraints on shading, height and surface smoothness. This algorithm was run on both synthetic and real SEM data.

In the following, we briefly summarize the advantages, disadvantages and limitations of each 3D SEM surface reconstruction strategy.

Single-View Methods

Pros:

(1) It only requires additional lighting.

(2) It can be easily implemented at an appropriate computational cost.

Cons:

(1) It is not able to create a whole 3D model since it only uses a single perspective.

(2) The obtained 3D models would be limited to only a particular view angle.

(3) Using standard SEM machines make it difficult to work using this approach.

Multi-View Methods

Pros:

(1) It can produce a better 3D model since it uses multiple images.

(2) Most SEM machines can produce images by tilting the specimen over different angles.

Cons:

(1) It requires more sophisticated algorithms and computational time.

Hybrid Methods

Pros:

(1) It takes advantages of both Single-View and Multi-View approaches.

Cons:

(1) It is not operational or cost effective with common SEM machines.

Based on the pros and cons of each 3D SEM surface reconstruction method illustrated in the above paragraph, in this work we will enhance the accuracy, reliability, and speed of 3D SEM surface reconstruction by a novel optimized, adaptive, and intelligent algorithm utilizing the Multi-View technique. As we have presented in the taxonomy (Figure 1.2), an optimized multi-view class of 3D SEM surface reconstruction has not yet been implemented, and it could be considered as a major part of our contributions. In addition, we will improve the general performance of the work using and adaptive and intelligent strategies.

1.5   Motivations and Objectives

The motivations of the proposed work are to revisit the state of the art in 3D SEM surface reconstruction techniques to provide a better understanding of the work, and integrating advanced 3D vision technologies into the SEM to:

- Create realistic anatomic shapes from microscopic samples.

- Allow rotation and depth for further interpretation of microscopic objects.

- Offer quantitative and visual information for a variety of applications in biology and material sciences.

1.6 The Main Contributions

Our goal is to design an optimized, adaptive, and intelligent multi-view method to calibrate SEM extrinsic parameters and reconstruct the 3D shape model in a fast, reliable, and accurate fashion. The major components of our work will be: (1) Using multi-view geometry to restore a 3D surface model from SEM micrographs. (2) Take a global optimization strategy into account to find the best fitness model for both SEM extrinsic calibration and its 3D surface structure. (3) Take statistical methodology along with artificial intelligence and machine learning advantages to develop an adaptive and intelligent 3D microscopy method. Our **main contributions** follow:

- An important contribution of the work would be introducing an exciting but challenging application area to the computer vision community. While 3D surface reconstruction from a set of 2D images in general has been studied for a long time in computer vision, the use of existing techniques in 3D microscopy vision and analysis of SEM images has been very limited so far. We will review the evolution of 3D SEM surface reconstruction systems, and discuss the success and failure of existing approaches to the problem. We will explain the state of the art algorithms adopted over the years in attempting to solve the 3D surface reconstruction from SEM images. The present work is expected to highlight the important roles and applications of 3D computer vision algorithms in the area of 3D microscopy vision, particularly 3D surface reconstruction from SEM images.

- We will present a taxonomy of several models, which provides a critical comparison of the current approaches, their capabilities and deficiencies, and conclude with some of the challenges that can be resolved with recent advances in 3D computer vision. We do hope that this work will serve as a guide for 3D SEM surface reconstruction.

- The main contribution of this research would be a novel integration of several computational technologies, including multi-view geometry, optimization algorithms, statistical approaches, and machine learning strategies into the estimation of SEM motion parameters and its 3D surface reconstruction. With the current work, we will design and develop a method to calibrate SEM extrinsic parameters and restore the 3D shape model in a fast, reliable, and accurate fashion.

- We initiate a study of an adaptive algorithm combined with supervised machine learning strategies and a global optimization platform for reconstructing 3D surface structures of SEM images. To the best of our knowledge, our work is the first attempt to design and develop an optimized, adaptive, and intelligent method for 3D SEM surface reconstruction.

- The last contribution of the work would be creating a 3D SEM surface reconstruction dataset, and make it publicly and freely available to the research community. The dataset, which will include both 2D SEM images and 3D surface models along with the underlying methodology, serves as a guide for 3D SEM surface reconstruction problem, leading to reproducible research in 3D microscopy vision. We also initiate the study of SaaS based architectures for essential 3D SEM surface reconstruction techniques. To the best of our knowledge, our work is the first attempt to design and develop a 3D microscopy dataset and a set of World Wide Web services for highly demanding 3D SEM surface reconstruction algorithms.

Chapter 2

3D Surface Reconstruction

In this section, an attempt will be made to discuss the different computational technologies involved in our proposed 3D SEM surface reconstruction system. We shall begin with the different parts of the methods to tackle the problem of the multi-view 3D SEM surface reconstruction problem in an optimized, adaptive, and intelligent fashion.

2.1 Multi-View Geometry

Multi-view geometry is established on the theory of projective geometry, considering different perspectives to restore the 3D structure of a specific object [33], [54], [84], [109], [125]. A basic requirement is the determination of camera's intrinsic and extrinsic parameters given as a 3×4 camera projection matrix. A homogenous 2D point $\widetilde{\mathbf{x}} \sim [\widetilde{x} \quad \widetilde{y} \quad \widetilde{w}]^\top$ and 3D point $\widetilde{\mathbf{X}} \sim [\widetilde{X} \quad \widetilde{Y} \quad \widetilde{Z} \quad \widetilde{W}]^\top$ (where $\sim$ means equality up to scale) are related to their Euclidean equivalents $\mathbf{x} = [x \quad y]^\top$ and $\mathbf{X} = [X \quad Y \quad Z]^\top$ by the following equations [33], [54]:

$$\mathbf{x} = [\widetilde{x}/\widetilde{w} \quad \widetilde{y}/\widetilde{w}]^\top \qquad\qquad \widetilde{\mathbf{x}} \sim [x \quad y \quad 1]^\top \qquad (2.1)$$

$$\mathbf{X} = [\widetilde{X}/\widetilde{W} \quad \widetilde{Y}/\widetilde{W} \quad \widetilde{Z}/\widetilde{W}]^\top \qquad\qquad \widetilde{\mathbf{X}} \sim [X \quad Y \quad Z \quad 1]^\top \qquad (2.2)$$

Letting P be a 3×4 projection matrix of the camera, a 3D point $\widetilde{\mathbf{X}}$ is related to its pixel position $\widetilde{\mathbf{u}}$ in a 2D image array by the following relationship:

$$\widetilde{u} = P\widetilde{\mathbf{X}} \qquad (2.3)$$
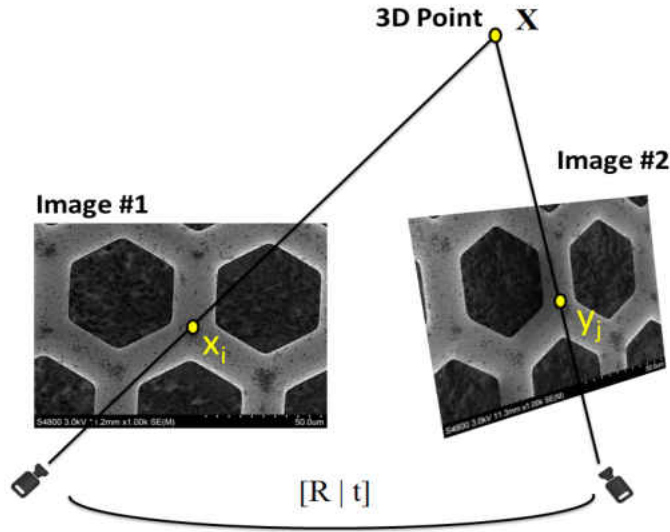
Figure 2.1: A 3D point X and its projected positions in images from two views. The projections of a point X onto the two images are denoted by x_i (image on the left) and y_j (image on the right).

The projection matrix P is typically in the form of A $[R \quad t]$, where A is a 3×3 matrix which encapsulates internal parameters of the camera that are required to register the pixel coordinates of an image with the corresponding coordinates in the camera's reference frame. Matrix A can convert $\mathbf{x}$ in the camera image plane to a pixel coordinate $\widetilde{u} = [u \quad v \quad 1]^\top$ by $\widetilde{u} = Ax$. R and t are known as the camera's extrinsic parameters that define the location and orientation of the camera reference frame with respect to a known world reference frame [54]. The 3×3 fundamental matrix, denoted by F, encapsulates the camera motion from image correspondences using SIFT [78], SURF [15] or other image feature detection algorithms. By considering a 3D point and its projected images in two different camera locations, if a point $\mathbf{X}$ in 3D space is imaged as x_i at the first view and y_j at the second view (Fig. 2.1), then the image points satisfy the equation (2.4). The equation (2.5) defines the constraint verification for equation (2.4) [33], [54], [125]:

$$y_j^\top F \, x_i = 0 \qquad (2.4)$$

16

$$F = A_2^{-\top} R \; [t] \; A_1^{-1} \qquad\qquad (2.5)$$

The two matrices A_1 and A_2 include the internal parameters of the first and second camera, respectively. The essential matrix is the matrix E that relates an image of a point in one camera to its image in the other camera given a translation and rotation (equation (2.6)).

$$E = A_2^\top F \; A_1 = R \; [t] \qquad\qquad (2.6)$$

From equation (2.3), we know that $x = PX$. By using equation (2.1), $x = w[u \quad v \quad 1]^\top$ where w is such a scale factor. If we have at least two 2D images from a specific object, and if we know P as a projection matrix, then we are able to recover $\mathbf{X} = (X, Y, Z, 1)^\top$ by least square method. Further information and recent progress on multiple view geometry can be found in [54].

In the case of multi-view 3D SEM surface reconstruction [114], the pipeline strongly requires image orientation estimation based on detected and matched feature points in the 2D SEM image set. The number of inliers corresponding points (True-Positive) as well as the number of outliers (False-Positive) has a serious impact on the quality of 3D shape reconstruction. While multi-view 3D surface modeling of SEM images usually employs globally-fixed thresholds, an adaptive and intelligent strategy will adapt thresholds to the input images and consequently it is able to detect more inliers, keeping away the outliers at the same time. The motivation of the current work is to improve the performance, accuracy, and reliability of 3D SEM surface reconstruction by maximizing True-Positive as well as minimizing False-Positive corresponding points simultaneously. To this end, we design and develop a novel framework which includes two distinctive quality attributes as follows:

(1) Optimized The third attribute of the proposed framework is to integrate a Differential Evolutionary (DE) strategy [25], [46] into the estimation of SEM extrinsic parameters and the 3D surface model to determine the best fitness model. It increases the reliability and speed of the 3D SEM surface reconstruction process.

(2) Adaptive As we mentioned earlier, feature points detection and points matching has a crucial impact on the quality of 3D SEM surface reconstructions. Since general 3D SEM surface reconstruction algorithms have only used constant and fixed thresholds to find the corresponding points, we will employ a statistical methodology namely *a Contrario* model estimation [37], [39], to adapt thresholds to input images for each image pair in the set. This attribute makes users free from manually trade off the thresholds or rely on the default configurations. Furthermore, it leads the system to increase the number of correct matches and consequently improves the accuracy and quality of 3D surface models.

(3) Intelligent Points matching requires comparing a large number of multi dimensional descriptor vectors (e.g., the SIFT algorithm [78] employs a vector of 128 elements). We apply a machine learning technique in which a binary supervised classifier will identify feature points that are useful for the matching processing step. This attribute speeds up and increases the accuracy of the matching process, and it potentially enables a decrease in the amount of false-positive corresponding points.

2.2 Differential Evolutionary Algorithm

The first component of our work is doing an optimization process by defining a cost function for any set of parameters (3D points and relative poses including extrinsic SEM parameters which specify rotation and translation from one view point to the other). We first estimate the rotation and translation from the set of corresponding points between two images in the image set. For this purpose we employ the highly used SIFT [78], [112], [131] algorithm along with KNN [10] to find the matching points in the image pair. We examined BRIEF [22], and SURF [16] feature detectors and eventually chose the SIFT algorithm base on our experiments illustrated in [110]. Then, we apply an iterative strategy called RANSAC [47], [54] to select the correct inlier points in the set of all corresponding points. We next take advantages of multi-view geometry to estimate the rotation and translation, and perform linear triangulation to initialize the 3D locations

of all matching points. The next step is a refinement process by defining a cost function for any set of parameters as to whether this is a good or bad set.

For the refinement, the most important part is to parameterize the space of rotation and translation. In order to have much simplicity and better flexibility, the quaternion parameterization [54] is applied to formulate the 3D rotation.

A quaternion $\mathbf{z} = a + bi + cj + dk$, where a, b, c, d are real numbers and $i^2 = j^2 = k^2 = -1$, and $\mathbf{z}$ is a unit quaternion if and only if [54]:

$$|z| = \sqrt{a^2 + b^2 + c^2 + d^2} = 1 \tag{2.7}$$

Then the rotation matrix representation is as follows [54]:

$$R(z) = \begin{bmatrix} a^2 + b^2 - c^2 - d^2 & 2bc - 2ad & 2bd + 2ac \\ 2bc + 2ad & a^2 - b^2 + c^2 - d^2 & 2cd - 2ab \\ 2bd - 2ac & 2cd + 2ab & a^2 - b^2 - c^2 + d^2 \end{bmatrix} \tag{2.8}$$

We define the translation vector of the second position with respect to the first one as $t = (t_x, t_y, t_z)^\top$. By considering the equation (2.8) for rotation parameterization and t for translation, then the parameterization of two projection matrices will be determined by a seven-dimensional vector $\theta = (a, b, c, d, t_x, t_y, t_z)^\top$. Now, SEM extrinsic calibration is equivalent to determining the parameter vector θ^* as in equation (2.9). In this equation, P is the SEM projection matrix which encapsulates rotation and translation (take a look at step (4) in Fig. 2.4).

$$\theta^* = \arg\min_{\psi}(\sum_{i=1}^{N} \|x_1^i - P(X_i)\|^2 + \|x_2^i - P(\psi, X_i)\|^2) \tag{2.9}$$

In generic 3D surface reconstruction, the iterative bundle adjustment algorithms [77] were frequently employed to solve this kind of equation. The bundle adjustment algorithms are among local minimizer (not global) techniques which suffer from different

problems. For instance, they commonly work on differential functions only and it is important to have an initial guess close to the real answer to converge [32], [99], [117]. In contrast to the traditional bundle adjustment approaches, the Differential Evolutionary (DE) algorithm [25], [35], [46], [107], [108] [113] is a global, population-based, and stochastic optimization strategy which does not tolerate these limitations and also is known as a fast evolutionary algorithm to optimize real number functions [52], [86]. DE as a genetic searching-based minimization algorithm uses generated populations within the parameter space. It first generates an initial population randomly, then iteratively updates them to estimate the best possible values for an optimization problem. The initial population is modified from one generation to the other by using two major operators: 1) Mutation, and 2) Crossover [25], [46]. The population generation process will be continued until a termination condition is met (i.e. number of generations). Here, we delve into the details of using the DE optimization strategy to solve the cost function illustrated in equation (2.9).

We define $\theta_{i,G}$ as the i-th parameter vector in the G-th generation by:

$$\theta_{i,G} = (a_{i,G}, b_{i,G}, c_{i,G}, d_{i,G}, t_{xi,G}, t_{yi,G}, t_{zi,G}) \tag{2.10}$$

Where i=$(1, 2, ..., P_{total})$, and G=$(1, 2, ..., G_{max})$ by assigning the size of population to $POPULATION_{total}$, and the maximum number of generations to G_{max}. We employ the mutation operator $p_{i,G} = \theta_{p,G} + S \times (\theta_{q,G} - \theta_{r,G})$ to produce deviation from one generation of a population to the next. $S \in [0, 2]$ and $\theta_{p,G}$, $\theta_{q,G}$, $\theta_{r,G}$ are three individual random agents in the population. The DE algorithm for solving the problem in equation (2.9) is described by the following Pseudo-code:

Algorithm 2.1. Proposed DE algorithm for 3D SEM surface reconstruction

Input: Matching points, initial SEM extrinsic parameters and 3D locations

Output: The best fitness of SEM extrinsic parameters and 3D points

```
begin
```

```
   Initialization:

  read S, CR, POPULATION_{Total}, G_{max};

  Initialize the population {θ_i;(1<=i<=POPULATION_{Total})} randomly;

  for (G=1; G < G_{max}; G ++)

    for (i=1; i<=POPULATION_{Total}; i++)

      Mutation and Crossover:

        choose three individual agents θ_{p,G}, θ_{q,G}, θ_{r,G} randomly;

          L = U(0,1);

          if L < CR

          p_{i,G} = θ_{p,G} + S × (θ_{q,G} − θ_{r,G})

        else

            p_{i,G} = θ_{i,G};

        if    p_{i,G} < θ_{i,G};

          θ* = p_{i,G};

      end.

    end.

 return   θ*

  end.
```

The parameters $CR \in [0, 1]$ and $S \in [0, 2]$ will be obtained by performing several experiments on the problem. We started with seven-dimensional parameter vector (θ^*) which is randomly assigned from the uniformly distributed numbers in the range (0,1) at generation G=1. During each generation (G+1), a new parameter vector including both rotation and translation parameters was then generated by adding the weighted difference vector between two population members to a third member. After G_{max} iterations ensuring convergence (G_{max}=1000 in our experiments) the population member θ^* with the highest confidence is considered to present the best solution.

2.3 The a contrario Methodology

As we discussed in Section 2.3, in generic multi-view 3D SEM surface reconstruction techniques, we have only employed fixed thresholds to distinguish the matching points in an image set. In practice, the matching step is often simplified to a specific and predefined threshold on the Euclidean distance to the nearest neighbor [78]. This is a serious issue, since the matching procedure is a major and preliminary step in multi-view 3D surface modeling. To tackle this issue, we need to utilize a system to discover a model which best fits the data with a confidence threshold that adapts automatically to different input images and possible noises as well. We employ the *a contrario* model estimation [40] to adapt thresholds to input images for each image pair in the set. The *a contrario* model estimation method was originally developed by Desolneux et al. [38], [40], [93], [120] to sort low level features in digital images. The approach assists us to detect sets of image feature points that are improbable, under a hypothesis that the visual features in given digital images are independent.

We begin with some principle notation. Suppose that two different views (Images I_1 and I_2) from the same microscopic sample are given. For every image, a feature detector and descriptor algorithm (e.g., the SIFT algorithm [78]) provides a set of keypoints with a static descriptor length, denoted by $(x_i, D(x_i))_{1 \leqslant i \leqslant N}$, and $(y_j, D(y_j))_{1 \leqslant j \leqslant M}$, where N and M are the numbers of detected feature points in I_1 and I_2 respectively. x_i and y_j are the coordinate vectors (e.g., pixel coordinates), and $D(x_i)$ as well as $D(y_j)$ are the corresponding feature descriptor vectors. Fig. 2.2 illustrates this situation in which there will be a 2D projective transformation H such that $y_j = H(x_i)$, and $x_i = H^{-1}(y_j)$.

The problem now is to discover a subset P of $\{1, 2, ..., N\} \times \{1, 2, ..., M\}$, and a homography transformation H such the two major following rules meet:

1. The distance between corresponding feature descriptors is below threshold δ_D, certifying that the local image features are very similar to each other:

$$\forall (i, j) \in P, d_D(D(x_i), D(y_j)) \leqslant \delta_D \tag{2.11}$$
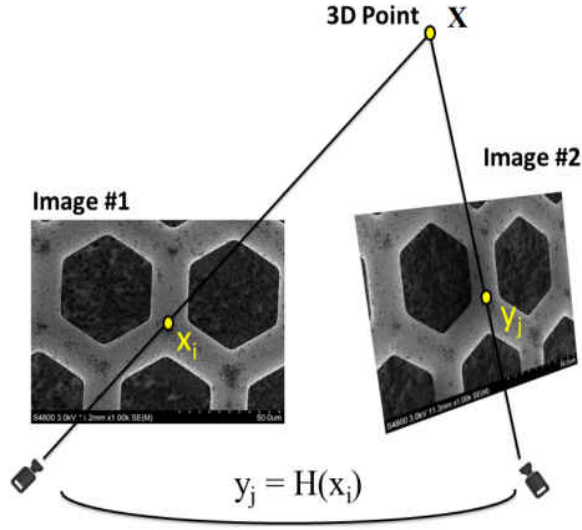
Figure 2.2: There is a 2D projective transformation H such that $y_j = H(x_i)$, and $x_i = H^{-1}(y_j)$.

2. The distance between two corresponding feature points is below the other threshold δ_G, ensuring that the constraint of homography transformation is satisfied:

$$\forall(i,j) \in P, d_G(x_i, y_j, H) := \max\{d_G(y_j, H(x_i)), d_G(x_i, H^{-1}(y_j))\} \leqslant \delta_G \qquad (2.12)$$

The *a contrario* methodology is able to automatically adapt and provide both thresholds δ_D and δ_G concerning different 2D SEM images and possible noises. Let's say a candidate feature point descriptor $D(x_i)$ is given, it would be matched with $D(y_j)$ if $d_D(D(x_i), D(y_j))$ is small enough under the assumption that all $D(y_j)$s from the set of feature points in image I_2 follow a random model namely background model, which we shall explain in the next paragraph. Considering the SIFT algorithm [78], we know that each descriptor $D(x_i)$ is made of K orientation histograms, $D(x_i) = (x_i^1, x_i^2, ..., x_i^K)$, and:

$$d_D(D(x_i), D(y_j)) = \sum_{k=1}^{K} d_D(x_i^k, y_j^k) \qquad (2.13)$$

where d_D is the earth mover's distance (EMD) between two histograms that well suits for circular histograms [36], [79], [93], [120]. Two feature point descriptors are then

23

more similar as distances between histograms are small enough. The background model would be any probabilistic paradigm on a feature descriptor $D(y)$ such that $\forall D(x_i)\ h_0$: $d_D(D(x_i^k, y^k)\ (k \in \{1, 2, ..., K\})$ are mutually independent random variables. In other words, the sets of feature points are said to be meaningful if their probability is very low under the hypothesis h_0 which states the feature points are mutually independent random variables [38], [93], [120]. The probability of the distance between $D(x_i)$ and $D(y)$ is smaller than δ_D could be evaluated as:

$$P\left(d_D(x_i, y) \leqslant \delta_D \,|h_0\right) = \int_{-\infty}^{\delta_D} *_{k=1}^{K}\ p_k^i(x)dx \qquad (2.14)$$

where $*$ is a convolution product and p_k^i denotes the density of random variable d_D as $d_D(D(x_i^m), D(y^m))$. For every $i \in \{1, 2, ..., N\}$ (image I_1) , and every $k \in \{1, 2, ..., K\}$, the rules p_k^i are experimentally calculated on $\{y_1, y_2, ..., y_M\}$ (image I_2). A correspondence between $D(x_i)$ and $D(y_j)$ in the set of feature points will be validated and it would be considered as meaningful as soon as the distance $\delta_D = d_D(D(x_i), D(y_j))$ is much smaller than the one expected under the hypothesis h_0 (e.g., as soon as the probability $P\left(d_D(x_i, y) \leqslant \delta_D \,|h_0\right)$ is quite small). As we have seen so far, for each feature point descriptor $D(x_i)$, it may not be an easy task to configure such a threshold as δ_{Di}. Utilizing *a contrario* strategy, the selection of these thresholds is substituted by a unique constraint on the expectation of the number of false alarms (NFA), that would be established in a handy way. For this purpose, the *a contrario* methodology introduces a function of $D(x_i)$ and δ_D as follows:

$$NFA\left(D(x_i), \delta_D\right) = N \times M \times P(d_D(x_i, y) \leqslant \delta_D \,|h_0) \qquad (2.15)$$

The *NFA* $\left(D(x_i), \delta_D\right)$ evaluates how likely that the distance between $D(x_i)$ and $D(y)$ is smaller than δ_D concerning the hypothesis h_0 on $D(y)$. Hence, a correspondence between $D(x_i)$ and $D(y_j)$ would be ε-meaningful if:

$$NFA\left(D(x_i), d_D(D(x_i), D(y_j))\right) \leqslant \varepsilon \qquad (2.16)$$

The following threshold will make it possible to confirm or refuse preferable correspondences between $D(x_i)$ and $D(y)$. A correspondence would be validated if $d_D(D(x_i), D(y_j)) \leqslant \hat{\delta_{Di}}(\varepsilon)$.

$$\hat{\delta_{Di}} = \arg\max_{\delta_D}\{NFA(D(x_i), \delta_D) \leqslant \varepsilon\} \qquad (2.17)$$

Fig. 2.3 visually shows the advantages of this strategy to improve the points matching process between two 2D SEM images.

2.4 Points Matching Using a Supervised Machine Learning Strategy

As we stated earlier, image points detection and matching have a great impact on the quality of multi-view 3D SEM surface reconstruction. The matching process of image features needs comparing a large number of multi dimensional descriptor vectors (e.g., the SIFT algorithm [78] utilizes a vector of 128 elements). Our goal in this section is to speed up and increase the accuracy of discovering corresponding points by classifying the extracted feature points in two major classes as follows:

- **Significant feature points**: These points are highly salient features, so matching between such feature points in different 2D SEM images is a great indicator of similarity.

- **Insignificant feature points**: These kind of points are less salient features, and they can not contribute visual similarities, so they could be operationally excluded from the matching process.

(A)

Original 2D Images

Image 1   Image 2

(B)

SIFT matching between two images

Image 1

Image 2

(C)

SIFT matching between two images using a contrario strategy
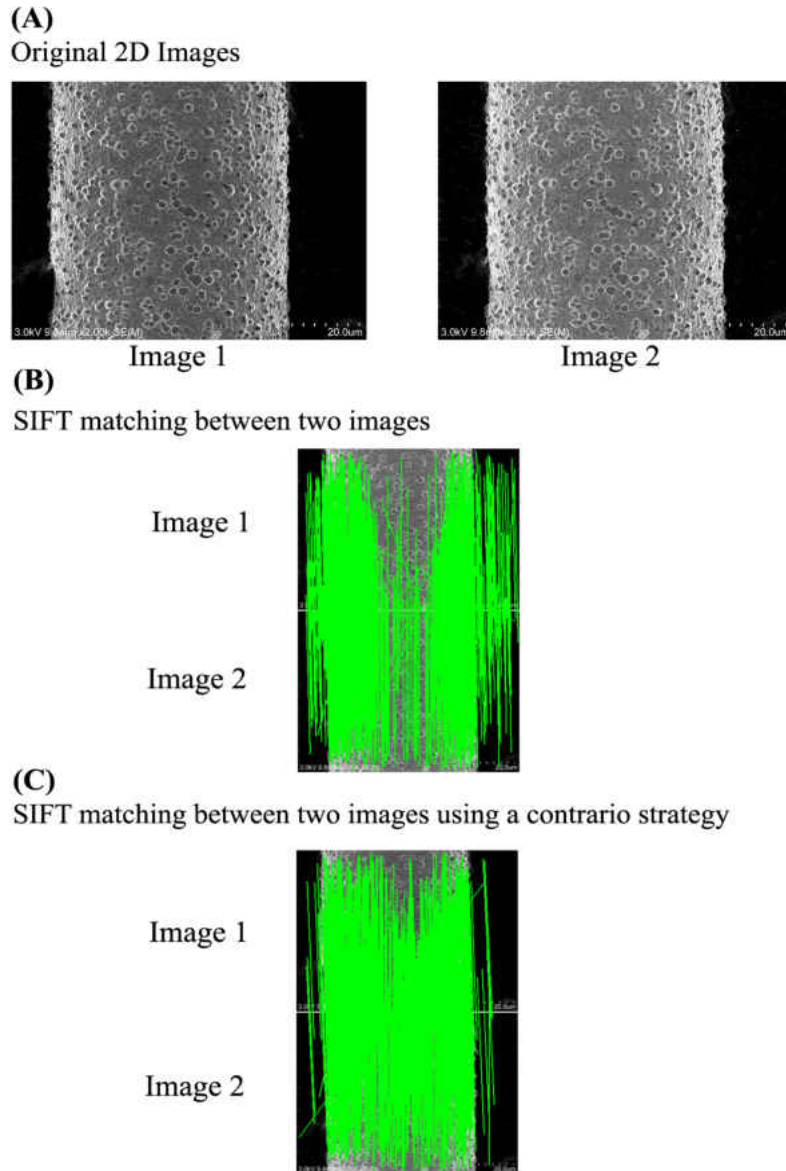
Image 1

Image 2

Figure 2.3: This figure illustrates the usefulness of the *a contrario* approach for the process of points matching. (A) Shows two SEM images from a TEM *copper grid bar*. (B) Shows the result of points matching using the SIFT algorithm. Only 2207 inliers have been detected. (C) Shows the results of points matching using SIFT algorithm plus *a contrario* strategy. Here, 3119 inliers have been detected. The green lines in (B) and (C) show all detected matching points including correct and incorrect ones.

In doing so, we make a binary classifier that can classify feature points from each other, identifying significant and insignificant points in a given dataset. Assume an input image I_1 is given. Using a feature detector algorithm, such as SIFT [78], a set of N feature points would be extracted from the given image I_1. Every feature point $n_i \in N$ can be described by a sequence of features F and denoted as $Q_F(n_i)$. In addition, assume that there is a classification function y which assigns a particular label for every feature point using the feature descriptor vector, such that:

$$y(Q_F(n_i)) \in C, \quad C = \{-1, 1\} \tag{2.18}$$

where -1 associates to the class of insignificant feature points, and 1 corresponds to the significant class. To make a classification function, a training dataset is required. A training instance for a feature point n is the tuple $n(x, y, Q_F(n_i), Class)$, such that x, y are the pixel coordinates for the feature point, $Q_F(n_i)$ is the feature vector, and $Class$ is the pre-defined category (e.g., significant or insignificant) of the feature point. Once the classification function has been learned, it can be utilized to determine the efficiency of a test feature point n' for the process of points matching.

We made a training dataset by utilizing a collection of 8 groups from a total of 41 2D SEM images including 167241 feature points [5], [115]. Each group consists of several SEM micrographs that are visually similar to each other, and they are captured by tilting the same specimen by different angles. Based on our previous experiences illustrated in [93], we employ the SIFT algorithm [78] along with KNN [10] and RANSAC strategies [47] to categorize the feature points in the training dataset. For each set of 2D SEM images, an image is randomly chosen and matched with the other images in the same group. A feature point is labeled as "significant" if it has a correspondence in at least one of the other images in the group. Other feature points that do not fulfill the condition, are then labeled as "insignificant".

In doing supervised machine learning, we examined four classification algorithms, namely Naive Bayes [81], [95], [115], Random Forest [13], [21], [59], Logistic Regression

27

[31], [49], [122], and Support Vector Machine (SVM) [17], [30], [63], [83] using the Weka software [53] which consists of a collection of easy-to-use machine learning algorithms in Java. We employed those components by their default and predefined settings established in the Weka 3.6 [4]. Based on the experiment that will be illustrated in Section 3.7, we eventually picked up the SVM classification algorithm to train and test the feature points data to know whether a point would be categorized as "significant" or "insignificant".

2.5 3DSEM++: An Optimized, Adaptive, and Intelligent 3D SEM Surface Reconstruction Approach

In this section, we put everything together to tackle the problem of 3D SEM surface reconstruction in an adaptive, intelligent, and optimized fashion. Fig. 2.4 shows the pipeline and block diagram of the proposed system.

We start with taking several 2D SEM micrographs by tilting the sample stage across different angles as shown in Fig. 3.1. This step requires SEM imaging configurations, such as magnification, working distance, etc. We then should detect and describe feature points in every single image in the image set, and discover the matching points. In doing so, we utilized very well-know algorithms, such as SIFT [78], SURF [15], ORB [100], and BRIEF [22], and eventually employed the SIFT algorithm based on our experiments illustrated in [110]. We then take the *a contrario* and supervised machine learning strategies explained in Section 2.3 and 2.4 into account to discover corresponding points between the images. Once we are done with that, we will estimate the image motion, the rigid body transformation from the first image to the next one using the corresponding points and epipolar geometry [54]. Having the relative positions of the SEM images, the 3D location of all matching points will be reconstructed by linear triangulation [54]. Finally, and for the purpose of finding the best fitness model, a global optimization technique namely Differential Evolution (DE) [25], [46] algorithm as illustrated in Section 2.2 will

(1) Take a set of SEM micrographs from different perspectives.

(2) Detect and describe features in every single SEM image.

(3) Features matching using the adaptive and intelligent strategies illustrated in Section 2.3 and 2.4.

(4) Estimate translation and rotation using multiple view geometry, and initialize 3D points by linear triangulation.

(5) Create the final 3D surface model using a global optimization process.

Figure 2.4: The pipeline of the proposed framework is shown in this figure. We begin the process with taking several 2D SEM micrographs by tilting the sample stage across different angles. This step requires SEM imaging style, such as magnification, working distance, and etc. We should detect and describe feature points in every single image in the set. Once we have done that, we will estimate the image motion, the rigid body transformation from the first image to the second one based on the matching points we have found in the image set. To identify a good enough number of inliers, we take adaptive and intelligent strategies illustrated in Section 2.3 and 2.4 into account. Once we estimate the relative position of the SEM images, the 3D position of all matching points would be reconstructed by linear triangulation. Finally, and for the purpose of finding the best fitness model, a global optimization technique called DE would be performed.

be performed.

Chapter 3

3D SEM Surface Reconstruction and Experimental Validation

In order to study and analyze the general performance, accuracy, and speed of the proposed system discussed in Chapter 2, extensive experiments on both real and synthetic data were carried out. In Section 3.1 and 3.2, an introduction to SEM imaging and biological sample preparation will be explained. In Section 3.3, we first introduce the test bed, experimental setup, and the dataset attributes. The qualitative 3D visualization results obtained by real microscopic samples are shown in Section 3.4. After that, in Section 3.5, we measure and compare the accuracy of our proposed framework to SEM extrinsic calibration using real microscopic samples along with the ground truth SEM rotation. In Section 3.6, we study the convergence rate of our proposed strategy with respect to different numbers of generations employed by the DE algorithm. Section 3.7 shows the validation summary for the prediction model. At the end of experimental validations, in Section 3.8 we further examine the quantitative validation and compare the system accuracy on 3D shape modeling and 3D rotation calibration by applying the proposed method on a set of synthetic data, namely "*Face*" models [90].

3.1   SEM Imaging

The SEM produces high-resolution micrographs by accelerating an electron beam downward, in a vacuum, within the instrument column through a series of electromagnetic lenses and apertures, which regulate the size and coherency of the beam down to a nanometer-scale focal point. The electron probe scans within a frame a raster, line by line, over the specimen surface via an oscillating magnetic field generated by an electromagnetic coil near the final lens of the column. Magnification is changed by adjusting

the length of the scan lines on the specimen. The rastering electron beam creates a volume of primary excitation within the sample which causes a variety of interactions between the electrons and the specimen, of which there are two main types: elastic and inelastic collisions. Elastic interactions represent high-energy electrons that are scattered by atomic nuclei in the sample, immediately redirecting out of the specimen without a loss of energy. These backscattered electrons (BSE) are highly useful in the study of the elemental composition of samples. In contrast, inelastic interactions occurring between the incident beam and loosely bound orbital shell electrons of the sample eject secondary electrons (SE) of significantly lower energy (0-50eV), which can be drawn in by a positively biased Everhart-Thornley detector, where they are converted to photons, amplified in a photomultiplier and converted to an electrical signal. Secondary electron signal has the advantage of providing high-resolution surface topography since their lower energy permits only near-surface interaction with the specimen. In an SE image, the brightness of a given pixel correlates to the sum of the detected secondary electrons emitted from the corresponding beam location on the surface of the specimen. The SE image is thus a topographic map of the specimen, formed by the variation in SE emission as the beam is scanned over the surface, where surface protrusions and features angled towards the detector produce the greatest SE yield [18], [20], [26], [48], [89].

A Hitachi S4800 field emission scanning electron microscope (FE-SEM) was used to produce the SEM micrographs in this contribution. It is equipped with a computer controlled, motorized goniometer stage capable of 5 axis of movement (x, y, z, tilt and rotation) controlled by Hitachi PC-SEM acquisition software. Samples were imaged at accelerating voltages of 3 or 5kv with emission current set to 10uA and normal probe current. For greatest signal, both upper and lower Everhart-Thornley SE detectors were utilized (Fig. 3.1). Working distance (z) was set to optimize depth of field for both maximum tilt and magnification used, and changes in working distance and magnification during the tilt series were compensated for automatically by the PC-SEM software. Brightness and contrast was manually adjusted for consistency between micrographs.
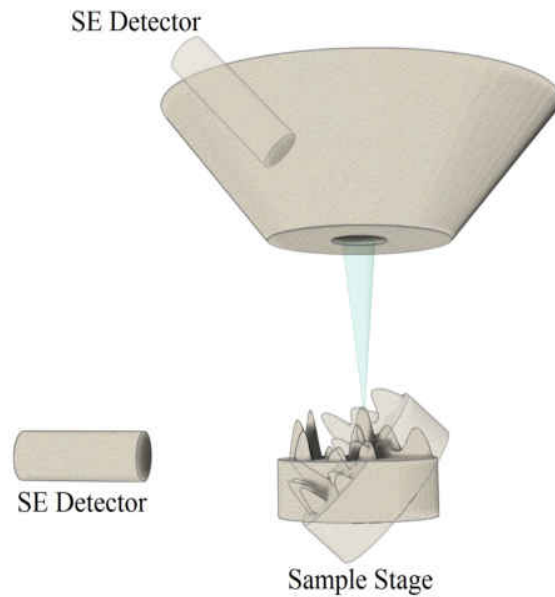
Figure 3.1: SEM imaging for the purpose of 3D SEM surface reconstruction.

3.2 Biological Sample Preparation for a SEM

With the advent of electron microscopy, novel ways to acquire specimens that were agreeable with the new technology were subsequently investigated. Among biologists, this means preserving the native structure of the sample without compromising the integrity of the vacuum or emission of electrons. Thus the vast majority of biological samples require a consistent methodology for preparation to be viewed by SEM. A generalized protocol for biological specimen preparation is as follows [26]:

1. **Fixation**: Immersion of specimen in chemical fixative to preserve natural structure of the sample. Examples: Glutaraldehyde, Formaldehyde and Paraformaldehyde.

2. **Rinse**: Removal of excess fixative and buffer salts with distilled water.

3. **Post-Fixation**: Further stabilizes sample and enhances conductivity.

4. **Rinse**: Removal of excess fixative and buffer salts with distilled water.

5. **Dehydration**: Removal of water from sample. Transitional fluids like carbon dioxide are not miscible with water.

6. **Critical Point Drying**: Drying sample with minimal deformation. Liquid carbon dioxide is commonly used.

7. **Specimen Mounting**: Specimen is mounted on a conductive stub. A variety of adhesives may be used depending on the nature of the sample.

8. **Specimen Coating**: A thin layer of conductive coating is applied to the sample through sputter coating or thermal evaporation. Examples: Gold, Platinum, Iridium, Chromium and Carbon. Metal alloys may also be used.

3.2.1 Chemical Fixation

The first step to preparing biological samples for electron microscopy is cross-linking molecules of the sample together the specimen without altering their natural structure and organization. Chemical fixation is a ubiquitous method of sample preservation that involves immersing the sample in a fixative [19]. The length of immersion is variable between specimens. Plant tissue, which comprises semi-impermeable barriers like cell walls or waxy cuticle on the tissue surface, require a longer immersion time for the fixative to fully infiltrate the sample. The relative thickness of the desired sample must also be taken into consideration when determining fixation time. It is also important to keep the specimen under optimal physiological conditions prior to and during fixation in order to reduce the possibility of creating artificial characters in the sample. Common groups of fixatives include aldehydes, heavy metals, and cold organic solvents. In some cases, a secondary fixation with a heavy metal is used to apply contrast, preserve membranes or enhance conductivity of the sample [26].

3.2.2 Dehydration

After the biological specimen has been preserved, the specimen is rinsed in water to remove excess buffer salts and unreacted fixative. This step is subsequently followed by the complete removal of all of the water from the sample. This is particularly important for maintaining the life-like state of sample because the removal of water reduces the pressure applied to the specimen surface during drying. Commonly, anhydrous organic solvents such as ethanol and acetone are used as an intermediate fluid to gradually remove any water present within the sample. Despite the fixation conducted previously, the sample is still susceptible to artificial characters like shrinking and extraction of internal elements. Ethanol, which is relatively gentle on the sample, is predominantly used during dehydration [26]. Acetone, by contrast, is a very effective solvent and capable to extracting lipidic compounds from the biological sample with relative ease. Due to the hygroscopic nature of anhydrous solvents, it is very important not to leave them exposed to the air for prolonged periods of time. Prolonged exposure can result in absorption of atmospheric water, rendering the dehydration process ineffective [19]. Dehydration of the sample is accomplished gradually through the incubation of increasing concentrations of the chosen solvent, culminating with several changes in 100% absolute solvent. As a general rule of thumb, the less amount of time spent in the dehydrating solutions, the better [26].

3.2.3 Drying the Sample

Although allowing the sample to air dry is an option, most microscopists forgo this choice due to the deformation that results. Most biological samples, when air dried, will exhibit a collapsed or distorted appearance. This artifact is a result of the surface tension forces associated with the interface between the liquid and gaseous states of the solvent. The pressure exerted on the sample can reach an excess of 2000 pounds per square inch (psi) when air drying, enough to easily destroy any fine or fragile features that may be present in the natural state. To avoid the destruction of the sample, a method known as

critical point drying (CPD) is commonly employed. CPD involves gradually replacing the dehydrant with a transitional fluid such as liquid carbon dioxide. Following the removal of the intermediate drying fluid, the chamber containing the specimen and transitional fluid is slowly heated to achieve a specific temperature and pressure. The temperature and pressure achieved depends on the transitional fluid used [19]. For liquid carbon dioxide, conditions of 31°C and 1073 psi are required to reach the critical point. At this point, the density of the liquid phase within and about the sample equals the density of the gaseous phase. This transitions the sample from being immersed in a fluid to immersion a dense vapor, thus avoiding any damaging effects from the liquid/gas interface. Upon achieving the critical point, the chamber remains heated while the vapor is slowly released until atmospheric pressure and the pressure within the chamber reach equilibrium [19].

3.2.4   Mounting and Conductivity

The dried specimen is then mounted a metal mount called a stub. Choosing the appropriate means of adhesion to the stub depends on a variety of factors. Is the sample large or small? Is the sample naturally conductive? Is orientation important for the sample? Methods for adhesion can range from a simple sticky tab to durable epoxy or cement [19]. Regardless of the method used, the sample must remain mechanically stable. It is important to choose a medium that will not damage the sample or compromise the vacuum of the instrument through out-gassing of solvents. Following adhesion of the sample to the stub, the sample is coated with a conductive material. Most biological specimens are not inherently conductive. As a result a coating of metal or carbon must be applied to reduce the chance of producing artificial characters that result from a buildup of electrons during imaging. The coating can be applied using an apparatus called a sputter coater or by thermal evaporation [19].

3.3 Experimental Setup

A Hitachi S-4800 Field Emission Scanning Electron Microscope was used to generate the micrographs for this study. This microscope is equipped with a computer controlled 5 axis motorized stage capable of 360 degrees of rotation with a tilt range of -5 to 70. Sample manipulation, such as tilt, Z-position, and rotation of the stage, as well as image processing and capture functions were operated through the Hitachi PC-SEM software. The working distance that would give the required depth of focus was determined at the maximum tilt for each specimen at the magnification chosen for image capture. As the sample was tilted in successive 1 increments through the software, the image was centered manually by moving the stage in the x- and y-axes with the stage positioning trackball. The working distance and magnification were kept consistent in each captured image of the tilt series by changing the Z-axis position as required. Brightness and contrast were manually adjusted for consistency between micrographs, using the same structure in each image. The micrographs were acquired with an accelerating voltage of 3 kV, utilizing the signals from both the upper and lower secondary electron detectors.

The proposed 3D SEM surface reconstruction system were implemented by Java2SE 8 and Matlab 2012a. We used 64-bit Windows 8 operating system on a PC with 3.00 GHz Intel Dual core CPU, 4MB cache and 6GB of RAM. Datasets names and attributes, SEM configurations, and initial parameters in our DE based algorithm are shown in Table 3.1.

3.4 Qualitative 3D Visualization

Six qualitative 3D visualization results using real microscopic samples are shown in Fig. 3.2 to Fig. 3.7. The first rows in these figures show a set of 2D images obtained from different perspectives. Their 3D point clouds, 3D surface meshes, and 3D shape models which were reconstructed by using our proposed method are also presented in the figures. The 3D geometric models presented here indicate that the proposed method is promising for 3D SEM surface reconstruction. By considering these results, it is evident that higher resolution SEM snapshots (SEM micrographs) improved the quality of the reconstruction

Table 3.1: Experimental setup and the dataset attributes. We used G=1000 (stopping condition for the DE algorithm) based on the experiments illustrated in Section 3.5 to satisfy both accuracy and the time efficiency. The initial population for the parameter space (θ) was generated as uniformly distributed random numbers in the range (0,1). The reason for choosing such a range is related to the common possible tilting angles in a SEM which is almost (0 to $\frac{\pi}{4}$) for our dataset.

Datasets	(1): *pollen grain* from *Brassica rapa*
	(2): TEM *copper grid*
	(3): *tapetal cell* of *Arabidopsis thaliana*
	(4): Hexagon TEM *copper grid*
	(5): Guitar String
	(6): TEM *copper grid* bar
Images attributes	(1): 854*640 grayscale, 512 dpi
	(2): 2560*1920 grayscale, 512 dpi
	(3): 2560*1920 grayscale, 512 dpi
	(4): 2560*1920 grayscale, 512 dpi
	(5): 5120*3840 grayscale, 1024 dpi
	(6): 1280*960 grayscale, 512 dpi
Rotation angle	(1): 3 degrees
	(2): 7 degrees
	(3): 9 degrees
	(4): 10 degrees
	(5): 4 degrees
	(6): 11 degrees
SEM detector	SE (mix) as shown in Fig. 3.1
SEM intrinsic parameters	A = [0.047 0 0; 0 0.047 0; 0 0 1]
DE parameters	$CR = 0.8$, $S = 0.9$
	$POPULATION_{Total} = 55$, $G_{max} = 1000$

process, although the computation time increased. Having more corresponding points and employing bigger rotation angles will also enhance the quality of the 3D reconstructed surfaces.

3.5 SEM Extrinsic Calibration

This section presents a validation summary on the reliability, accuracy, and time efficiency of the proposed strategy for SEM rotation estimation. We present various experimental results performed on multiple datasets illustrated in Table 3.1. We were given the rotation angles, but rotation axis and translation vector were unknown. A 3D rotation is a kind of rotation about one of the axes of a coordinate system. The following 3D rotation matrices (R_x, R_y, and R_z) rotate vectors by an angle θ about the x, y, and z axis, in three dimensions [54]:

$$R_x(\theta) = \begin{bmatrix} 1 & 0 & 0 \\ 0 & \cos\theta & -\sin\theta \\ 0 & \sin\theta & \cos\theta \end{bmatrix} \tag{3.1}$$

$$R_y(\theta) = \begin{bmatrix} \cos\theta & 0 & -\sin\theta \\ 0 & 1 & 0 \\ \sin\theta & 0 & \cos\theta \end{bmatrix} \tag{3.2}$$

$$R_z(\theta) = \begin{bmatrix} \cos\theta & -\sin\theta & 0 \\ \sin\theta & \cos\theta & 0 \\ 0 & 0 & 1 \end{bmatrix} \tag{3.3}$$

By using only two images in each set and setting the maximum number of DE generations to 1000, we got a rotation matrix R_1 and translation vector t_1 for the *pollen grain*
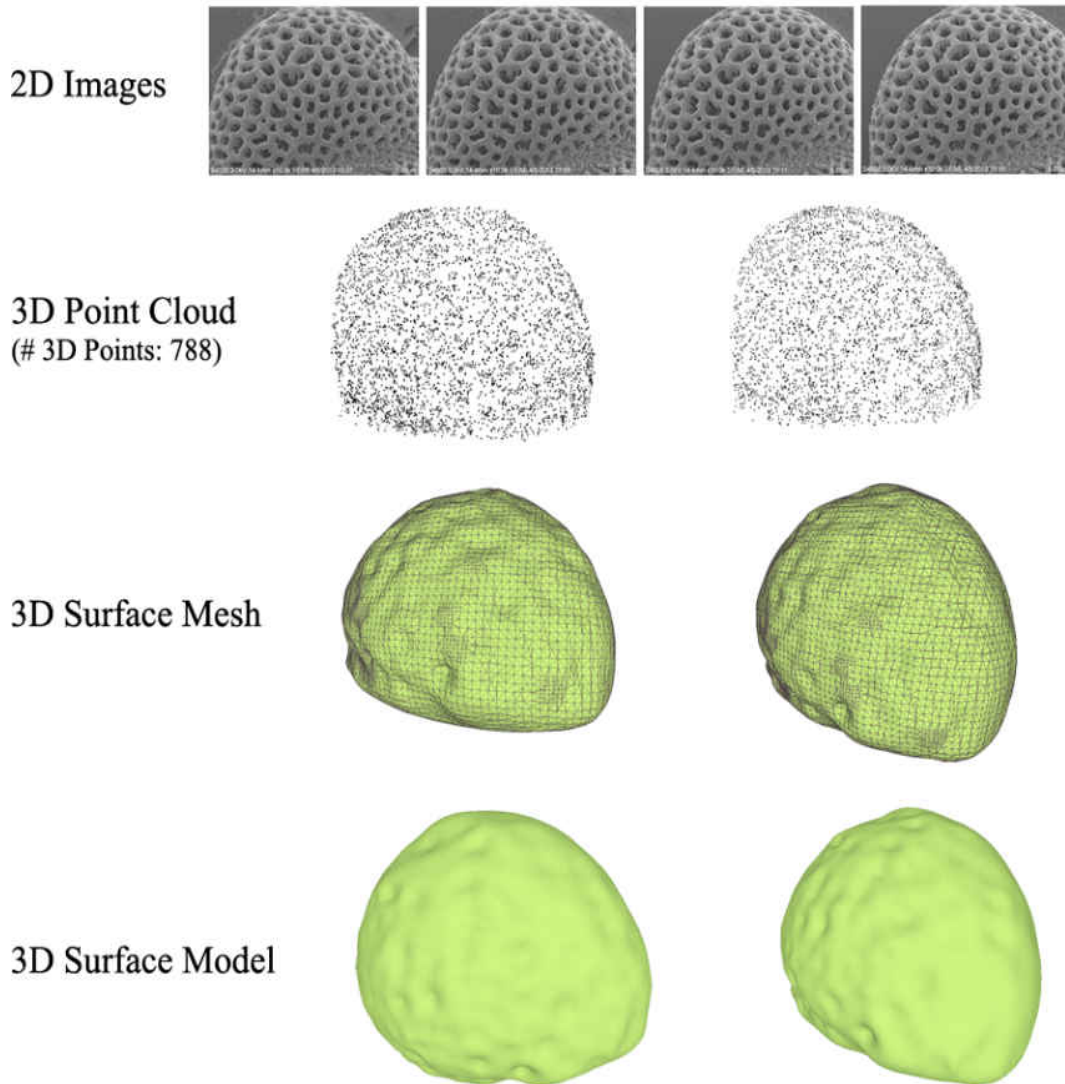
Figure 3.2: Qualitative visualization of 3D SEM surface reconstruction. This figure shows 2D SEM images, 3D point clouds, 3D reconstructed surface meshes, and surface models of a *pollen grain* from *Brassica rapa*. We present 3D point clouds, 3D surface meshes and the shape models from different perspectives. 2D images were obtained by tilting the specimen stage 3 degrees from one to the next in the image sequence. The attributes of these 2D images are illustrated in Table 3.1.
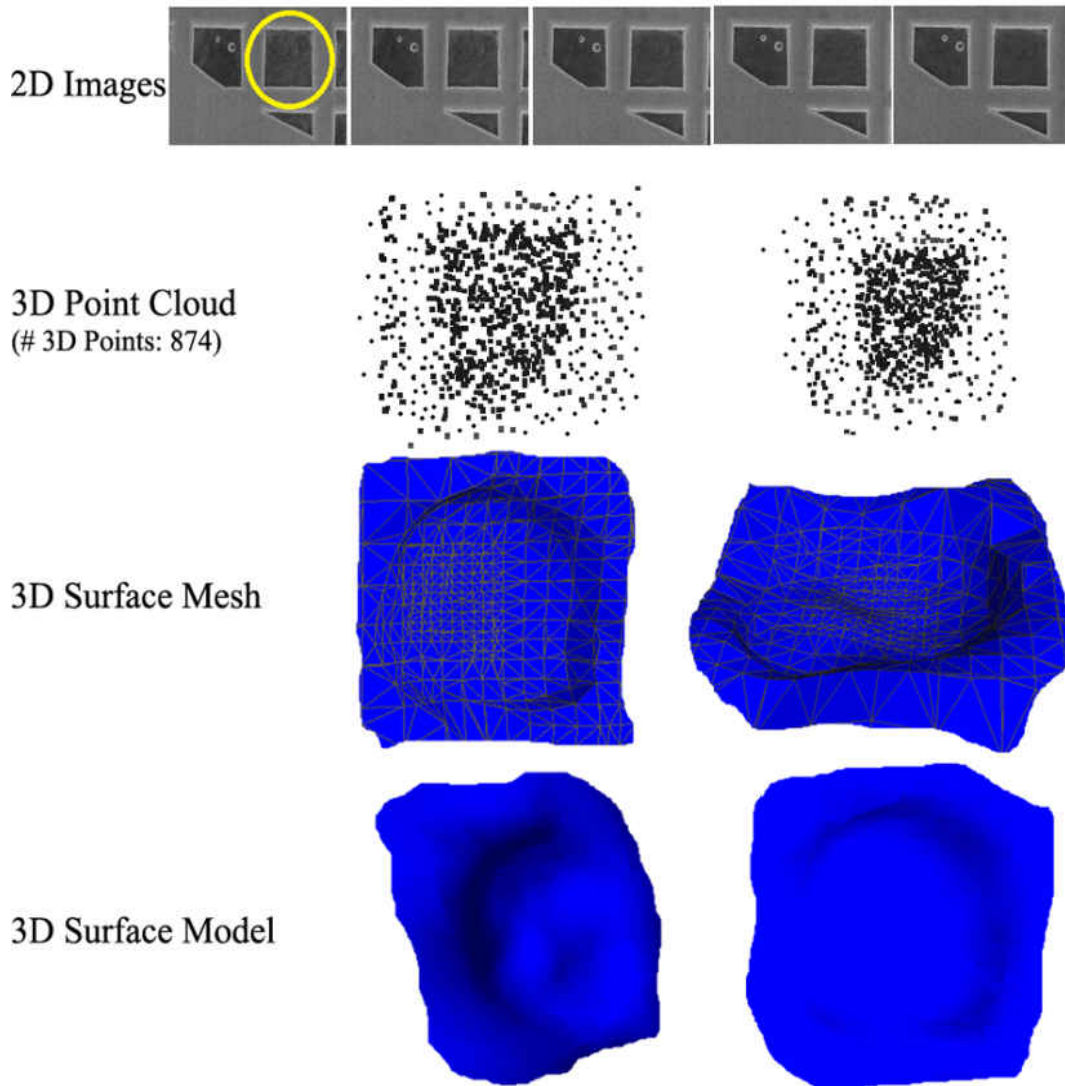
Figure 3.3: Qualitative visualization of 3D SEM surface reconstruction. In this figure, we present 2D SEM images, 3D point clouds, 3D surface meshes, and 3D shape models of a part of a TEM *copper grid* specified by the yellow circle in the first 2D image (at the first rows). We show 3D point clouds, 3D surface meshes and the shape models from different views. The 2D images were taken by tilting the TEM *copper grid* 7 degrees from one to next in the sequence. The attributes of these 2D images are presented in Table 3.1.
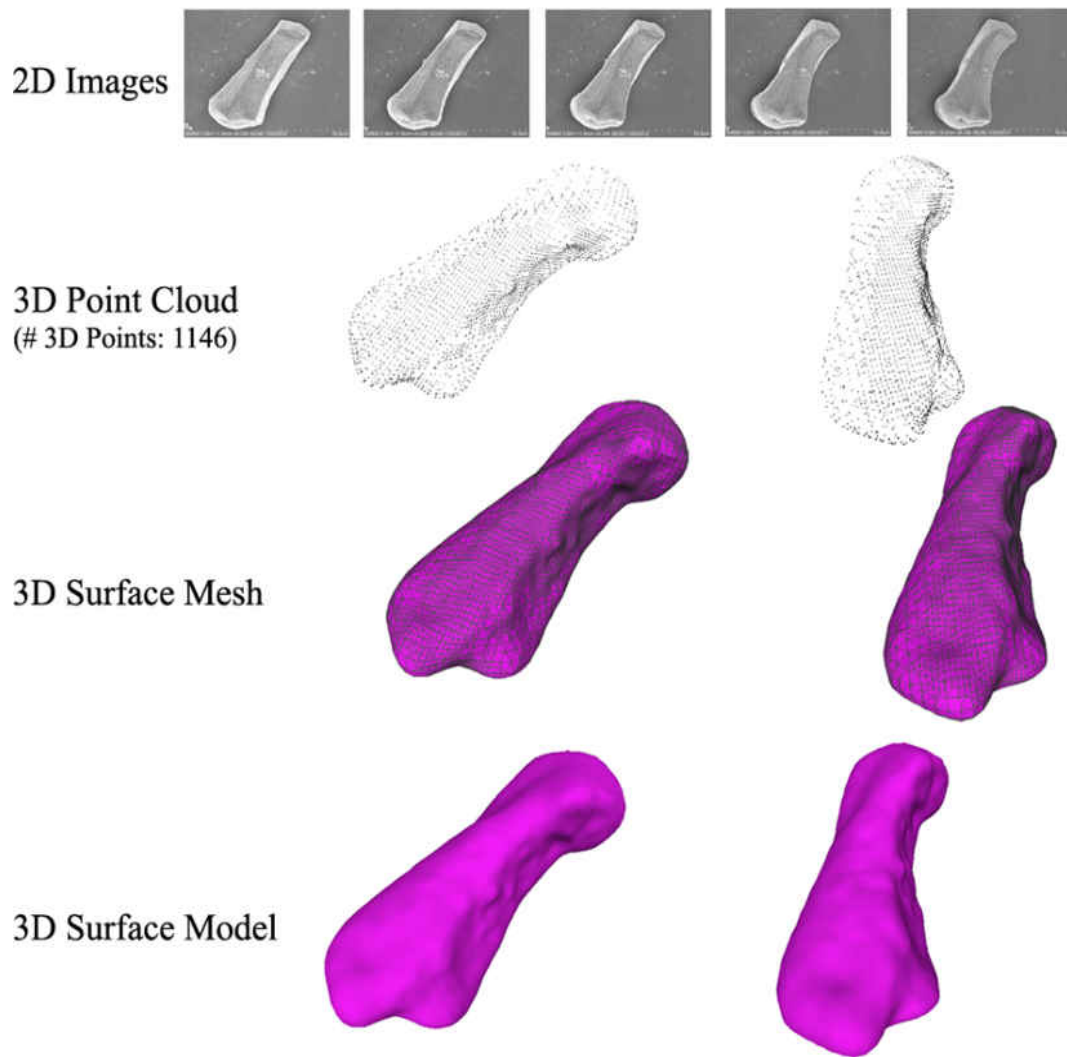
Figure 3.4: Qualitative visualization of 3D SEM surface reconstruction. The figure shows 2D SEM images, 3D point clouds, 3D surface meshes, and 3D reconstructed surfaces of a *tapetal cell* of *Arabidopsis thaliana* from different views. These images were obtained by tilting the specimen stage 9 degrees from one to the next in the image set. The attributes of these 2D images are shown in Table 3.1.
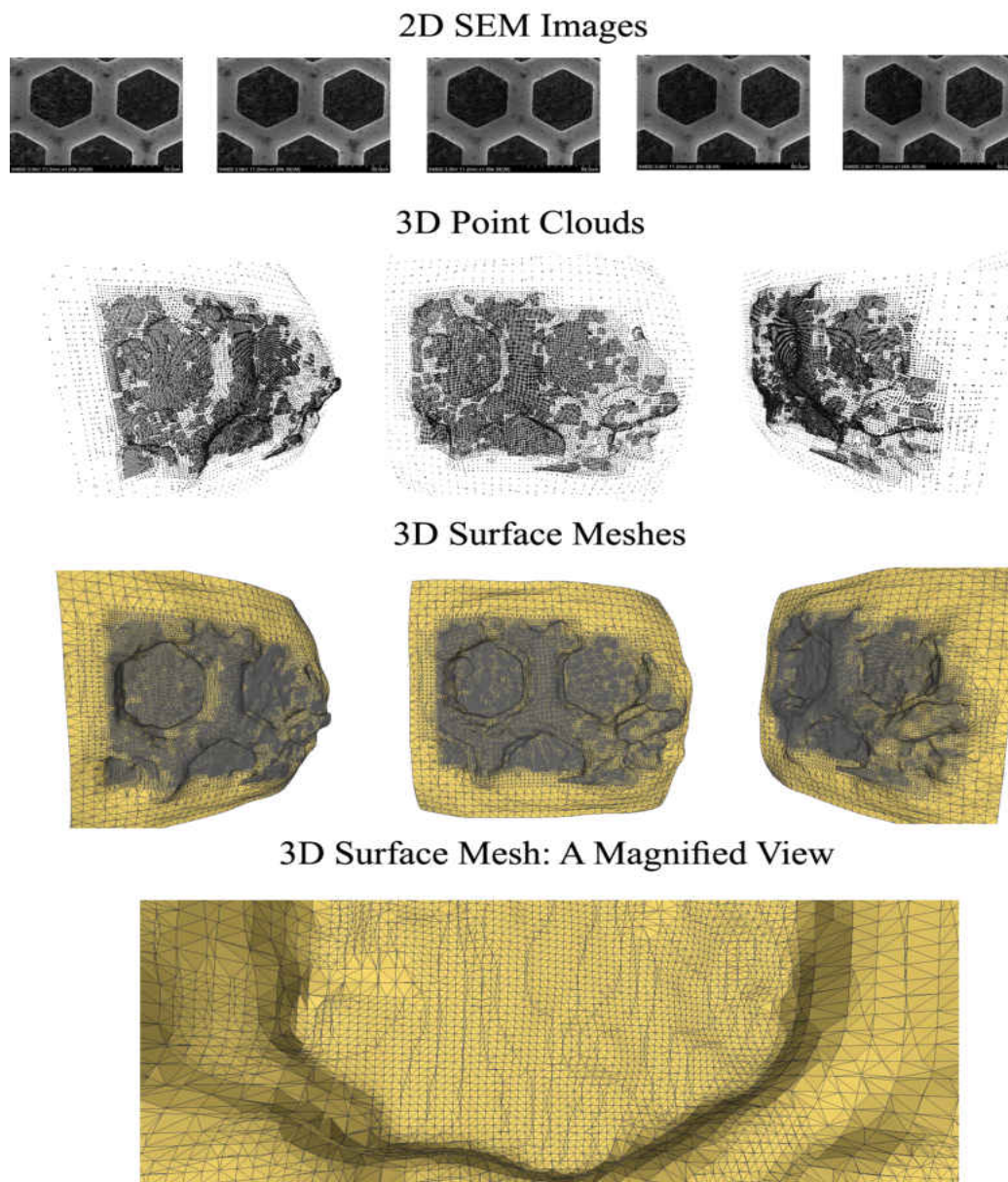
Figure 3.5: Qualitative visualization of the proposed 3D SEM surface reconstruction framework. This figure shows 2D SEM images, 3D point clouds, 3D surface meshes, and a magnified view of a Hexagon TEM *copper grid*. These images were obtained by tilting the specimen stage 10 degrees from one to the next in the image sequence. The number of point clouds are 37829. The attributes of these 2D images are shown in Table 3.1.
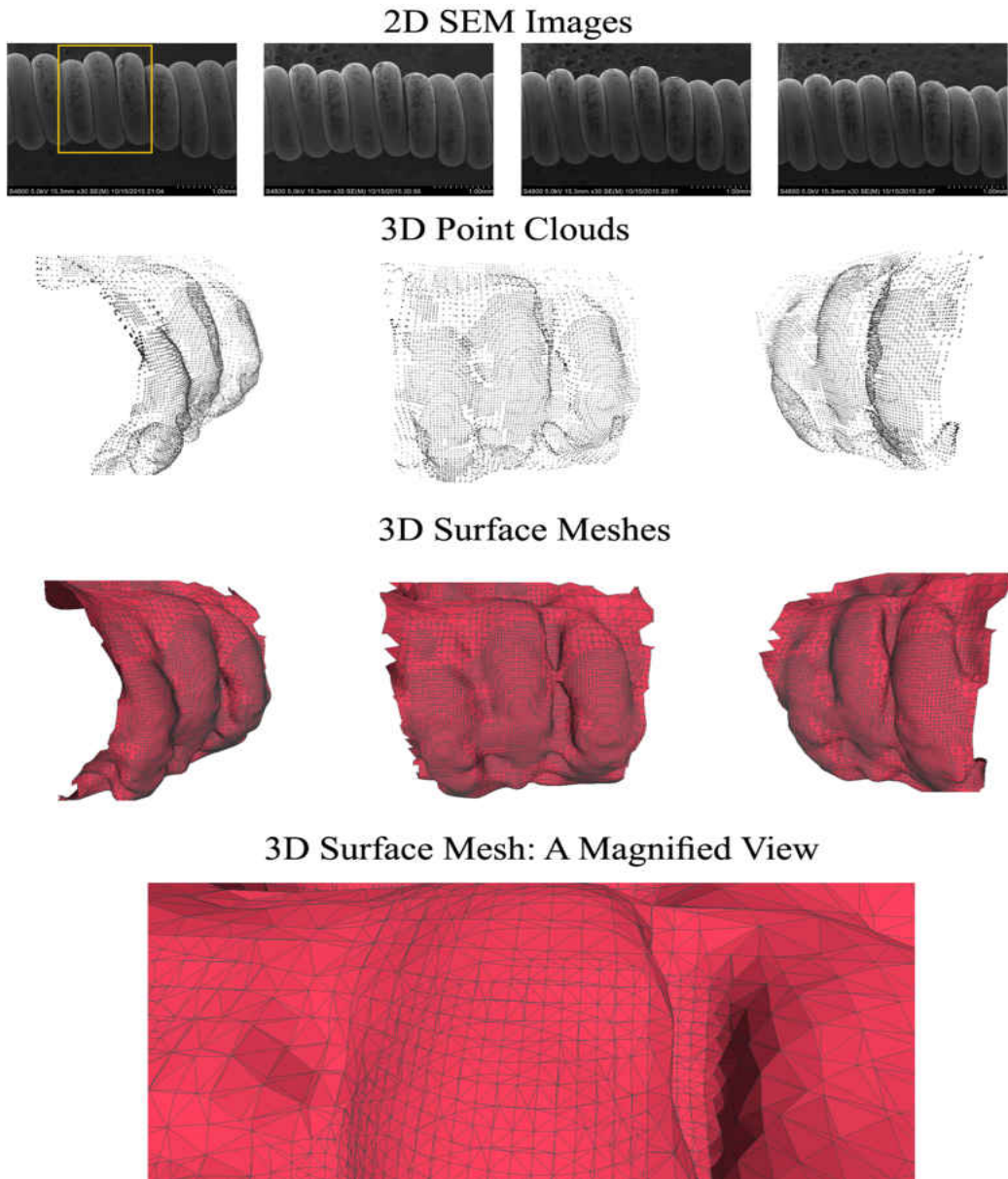
Figure 3.6: Qualitative visualization of the proposed 3D SEM surface reconstruction framework. This figure shows 2D SEM images, 3D point clouds, 3D surface meshes, and a magnified view of a Guitar String. These images were obtained by tilting the specimen stage 4 degrees from one to the next in the image sequence. The yellow rectangle specifies a part of the specimen which will be 3D reconstructed by the proposed method described in Section 2. The number of point clouds are 17228. The attributes of these 2D images are shown in Table 3.1.
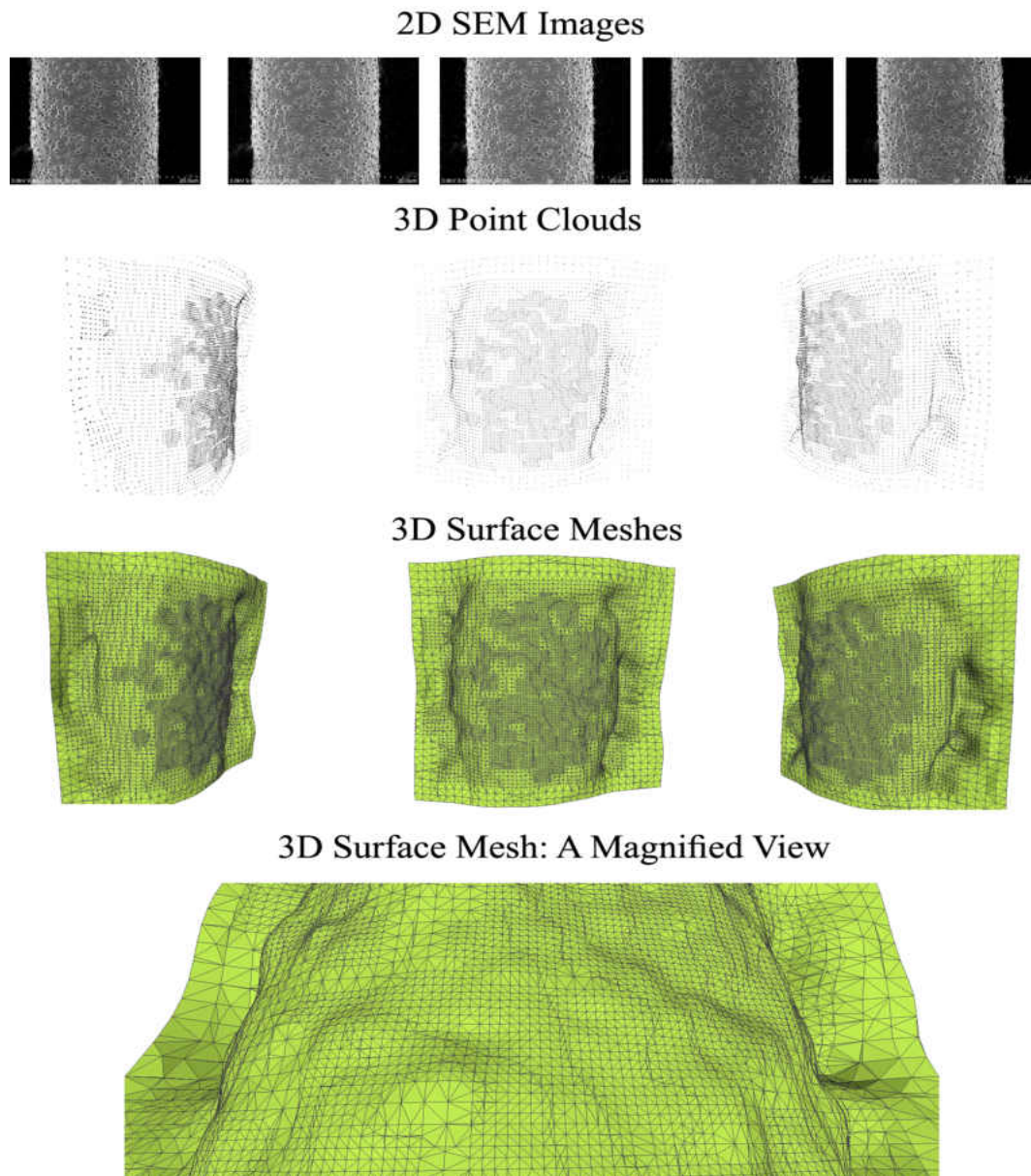
Figure 3.7: Qualitative visualization of the proposed 3D SEM surface reconstruction framework. This figure shows 2D SEM images, 3D point clouds, 3D surface meshes, and a magnified view of a TEM *copper grid* bar. These images were obtained by tilting the specimen stage 11 degrees from one to the next in the image sequence. The number of point clouds are 8811. The attributes of these 2D images are shown in Table 3.1.

from *Brassica rapa* (tilting by 3 degrees), R_2 and t_2 for the TEM *copper grid* (tilting by 7 degrees), R_3 and t_3 for the *tapetal cell* of *Arabidopsis thaliana* (tilting by 9 degrees), R_4 and t_4 for Hexagon TEM *copper grid* (tilting by 10 degrees), R_5 and t_5 for Guitar String (tilting by 4 degrees), and R_6 and t_6 for TEM *copper grid* bar (tilting by 11 degrees) as follows:

$$R_1 = \begin{bmatrix} 1.0000 & 0.0004 & 0.0001 \\ 0.0007 & 0.9948 & -0.1200 \\ 0.0011 & 0.1200 & 0.9948 \end{bmatrix} \tag{3.4}$$

$$R_2 = \begin{bmatrix} 1.0000 & 0.0001 & 0.0014 \\ 0.0008 & 0.9849 & -0.1407 \\ 0.0016 & 0.1407 & 0.9849 \end{bmatrix} \tag{3.5}$$

$$R_3 = \begin{bmatrix} 1.0000 & 0.0005 & 0.0015 \\ 0.0000 & 0.9835 & -0.1648 \\ 0.0007 & 0.1648 & 0.9835 \end{bmatrix} \tag{3.6}$$

$$R_4 = \begin{bmatrix} 1.0000 & 0.0007 & 0.0004 \\ 0.0009 & 0.9841 & -0.1654 \\ 0.0006 & 0.1654 & 0.9841 \end{bmatrix} \tag{3.7}$$

$$R_5 = \begin{bmatrix} 1.0000 & 0.0003 & 0.0000 \\ 0.0011 & 0.9941 & -0.1211 \\ 0.0024 & 0.1211 & 0.9941 \end{bmatrix} \tag{3.8}$$

$$R_6 = \begin{bmatrix} 1.0000 & 0.0001 & 0.0007 \\ 0.0004 & 0.9839 & -0.1663 \\ 0.0004 & 0.1663 & 0.9839 \end{bmatrix} \tag{3.9}$$

$$t_1 = [0.10073 \ \ 0.0019 \ \ 0.0029] \tag{3.10}$$

$$t_2 = [0.2164 \ \ 0.1003 \ \ 0.0017] \tag{3.11}$$

$$t_3 = [0.3727 \ \ 0.1020 \ \ 0.0002] \tag{3.12}$$

$$t_4 = [0.3733 \ \ 0.1000 \ \ 0.0004] \tag{3.13}$$

$$t_5 = [0.1011 \ \ 0.0023 \ \ 0.0001] \tag{3.14}$$

$$t_6 = [0.3739 \ \ 0.0043 \ \ 0.0016] \tag{3.15}$$

Reviewing 3D rotation matrices (equations 3.1, 3.2, and 3.3), we can claim that the rotation axis is the X axis. Various analysis from different angles in images and different numbers of DE generations (G_{max}) are presented in Table 3.2. The 3D rotation estimation error (ΔR) ranges from 4.98E-04 to 5.80E-03, mostly depending on the G_{max}. ΔR has been estimated using the equation (3.16):

$$\Delta R(R_{real}, R_{estimated}) = \sqrt{\sum_{i=1}^{n} \sum_{j=1}^{n} (R_{real(i,j)} - R_{estimated(i,j)})^2} \qquad (3.16)$$

It is evident that the reliability and the robustness of our approach remains acceptable by using different rotation angles, different images, and a varying number of matching points. We did not perform ground truth evaluation for the translation vector. However our estimation for translation values appear to have worked for 3D SEM surface reconstruction.

We have also compared the experimental results of our proposed approach with two other traditional approaches; namely ADBA (Algebraic Distance Bundle Adjustment) and ASDBA (Adaptive Sampson Distance Bundle Adjustment) [8], [118], [119] (Table 3.3). Elapsed times in Table 3.2 indicate only SEM extrinsic calibration. A graphical comparison of 3D reconstructed surfaces of *tapetal cell* of *Arabidopsis thaliana* using ADBA, ASDBA, and DE techniques is shown in Fig. 3.8.

3.6 Convergence Rate of the Proposed System

In this section we analyze the convergence rate of our proposed framework with respect to different numbers of generations (G_{max}) in Algorithm 2.1. The graphical comparisons are presented in Fig. 3.9. In this experiment we only use two images tilted by 3 degrees with 749 3D points for *pollen grain*, 7 degrees with 830 point clouds for TEM *copper grid* and 9 degrees with 509 3D points for *tapetal cell* set. The experiment clearly demonstrates that the proposed model has a stable convergence behavior with respect to the different numbers of generations and different 2D images.

3.7 Accuracy of the Prediction Model

In Section 2.4, we proposed a supervised machine learning approach to make a prediction model, knowing whether a feature point could be considered as "significant" or "insignif-

icant" for points matching. Here, a validation summary on the proposed supervised prediction model is established. In the sense of machine learning strategies, accuracy, precision, and recall are three common ways to analyze a prediction model, where accuracy refers to what percent of the predictions are correct, precision means what percent of positive predictions are correct, and recall refers to what percent of positive cases are detected [83], [115]. Table 3.4 shows the quantitative results for accuracy, precision, and recall of the proposed prediction model. These values has been calculated as the following equations [83], [115]:

$$Accuracy = \frac{True\,Positive + True\,Nagative}{True\,Positive + True\,Negative + False\,Positive + False\,Negative}$$

$$(3.17)$$

$$Precision = \frac{True\,Positive}{True\,Positive + False\,Positive} \tag{3.18}$$

$$Recall = \frac{True\,Positive}{True\,Positive + False\,Negative} \tag{3.19}$$

Our training and testing dataset includes a collection of 8 groups from a total of 41 2D SEM images containing 167241 feature points. For further examining the prediction models, we also examined the Receiver Operating Characteristic (ROC) and Area Under the Curve (AUC) [83], [115] for qualitative comparison of prediction models described in Section 2.4. ROC is able to illustrate the performance of a classification algorithm. The AUC was measured by the area under the ROC curve. Fig. 3.10 shows the ROC curve of our prediction models. The area of SVM classifier represented a reasonable test, and the areas of Logistic Regression and Naive Bayes classifiers were not good enough comparing to the other classification strategies. The accuracy of the SVM classifier on our datasets was working better than the Logistic Regression, Naive Bayes, or even Random Forest.
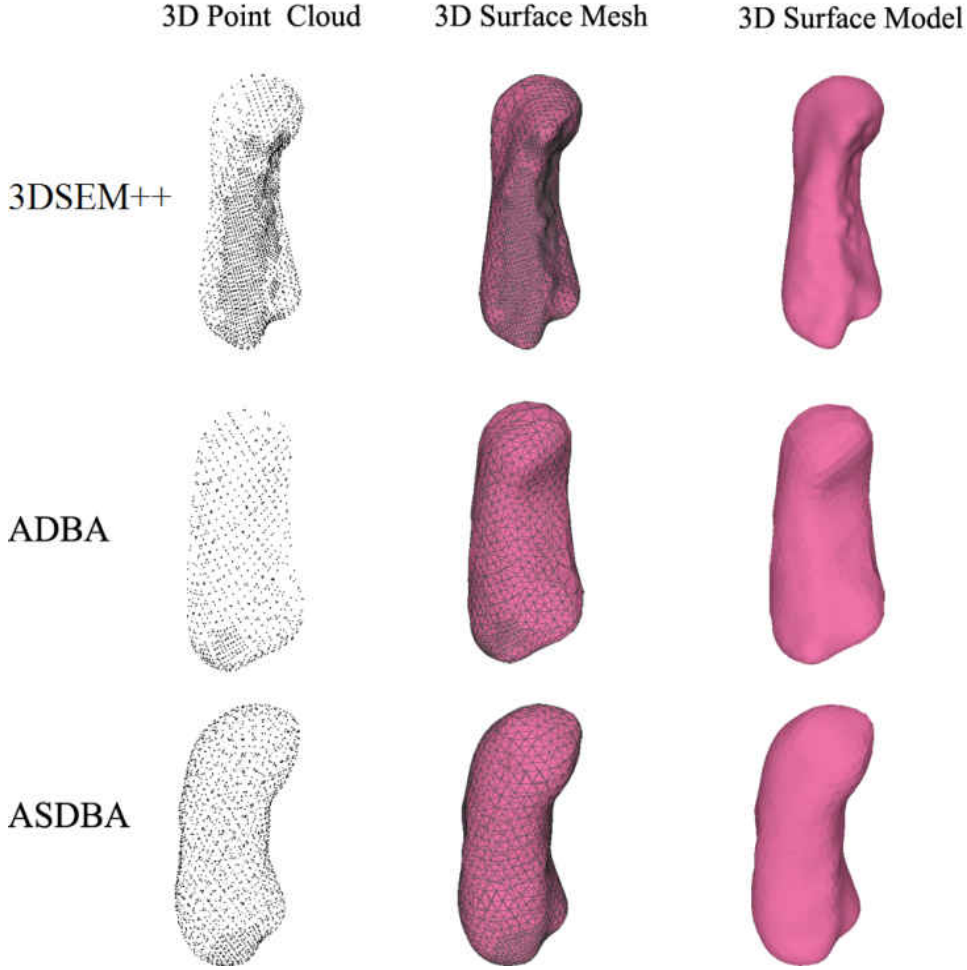
Figure 3.8: A graphical comparison of 3D reconstructed surfaces of *tapetal cell of Arabidopsis thaliana* using 3DSEM++, ADBA, and ASDBA techniques. We labeled our proposed method as 3DSEM++. The graphical comparison shows that our proposed optimized, adaptive, and intelligent strategy would be able to provide a better and detailed 3D surface model. Further quantitative comparisons are illustrated in Table 3.2 and Table 3.3.

Therefore, we selected the SVM algorithm for making a prediction model on the feature points dataset.

3.8 Quantitative Validation and Comparison

In this experiment, we further analyze the accuracy and reliability of the proposed approach for 3D SEM surface reconstruction. In doing so, the proposed system has been applied on four synthetic 3D "*Face*" models [90] to quantitatively compare the accuracy of the method with those two traditional methods mentioned in Section 3.5. We utilized Meshlab [2] to simulate the rotation angle using the synthetic face models. In doing so,

Table 3.2: Accuracy and reliability validation of our proposed method by examining different variables including the number of generations for the DE algorithm. ΔR is given as $R_{real} - R_{estimated}$ (equation 3.16), indicating error for estimating the 3D rotation. Rotation angles show the ground truth 3D SEM rotations (R_{real}). In each row we used only two images in the set. The elapsed times in this table indicate only SEM extrinsic calibration.

Image set	Total Matches	Rotation angle	G_{max}	ΔR	Elapsed time
pollen grain	761	3 degrees	500	4.26E-03	10.12 Sec.
pollen grain	761	3 degrees	1000	8.31E-04	12.05 Sec.
pollen grain	761	3 degrees	1250	5.54E-04	13.26 Sec.
pollen grain	689	6 degrees	500	4.68E-03	8.96 Sec.
pollen grain	689	6 degrees	1000	8.81E-04	9.59 Sec.
pollen grain	689	6 degrees	1250	6.65E-04	10.15 Sec.
pollen grain	634	9 degrees	500	5.63E-03	8.01 Sec.
pollen grain	634	9 degrees	1000	8.87E-04	9.11 Sec.
pollen grain	634	9 degrees	1250	7.07E-04	9.72 Sec.
TEM *copper grid*	849	7 degrees	500	3.07E-03	13.97 Sec.
TEM *copper grid*	849	7 degrees	1000	7.91E-04	15.30 Sec.
TEM *copper grid*	849	7 degrees	1250	7.11E-04	16.81 Sec.
TEM *copper grid*	731	14 degrees	500	4.53E-03	9.94 Sec.
TEM *copper grid*	731	14 degrees	1000	8.57E-04	11.71 Sec.
TEM *copper grid*	731	14 degrees	1250	7.03E-04	12.08 Sec.
TEM *copper grid*	670	21 degrees	500	5.80E-03	9.81 Sec.
TEM *copper grid*	670	21 degrees	1000	8.91E-04	10.73 Sec.
TEM *copper grid*	670	21 degrees	1250	6.02E-04	11.88 Sec.
tapetal cell	546	9 degrees	500	2.11E-03	5.98 Sec.
tapetal cell	546	9 degrees	1000	5.01E-04	9.13 Sec.
tapetal cell	546	9 degrees	1250	4.98E-04	9.60 Sec.
tapetal cell	468	18 degrees	500	2.54E-03	6.51 Sec.
tapetal cell	468	18 degrees	1000	7.10E-04	8.87 Sec.
tapetal cell	468	18 degrees	1250	6.83E-04	9.16 Sec.
tapetal cell	423	27 degrees	500	2.82E-03	5.17 Sec.
tapetal cell	423	27 degrees	1000	7.47E-04	7.64 Sec.
tapetal cell	423	27 degrees	1250	6.98E-04	8.33 Sec.

Table 3.3: Comparison of the proposed optimized, adaptive, and intelligent method with two other traditional strategies namely ADBA and ASDBA. The elapsed times in this table indicate only SEM extrinsic calibration. We labeled our proposed method as 3DSEM++. ΔR is given as $R_{real} - R_{estimated}$ (equation 3.16), indicating error for estimating the 3D rotation.

Image set	Method	Total Matches	Rotation angle	ΔR
pollen grain	ADBA	749	3 degrees	7.59E-02
	ASDBA	749	3 degrees	6.13E-02
	3DSEM++	761	3 degrees	**8.31E-04**
	ADBA	673	6 degrees	4.17E-02
	ASDBA	673	6 degrees	3.09E-02
	3DSEM++	689	3 degrees	**8.81E-04**
TEM *copper grid*	ADBA	830	7 degrees	3.88E-02
	ASDBA	830	7 degrees	3.03E-02
	3DSEM++	849	7 degrees	**7.91E-04**
	ADBA	722	14 degrees	6.17E-02
	ASDBA	722	14 degrees	4.44E-02
	3DSEM++	731	14 degrees	**8.57E-04**
tapetal cell	ADBA	509	9 degrees	7.39E-02
	ASDBA	509	9 degrees	9.86E-03
	3DSEM++	549	9 degrees	**5.01E-04**
	ADBA	441	18 degrees	2.41E-02
	ASDBA	441	18 degrees	5.19E-03
	3DSEM++	468	18 degrees	**7.47E-04**
Hexagon TEM *copper grid*	ADBA	15792	10 degrees	5.18E-04
	ASDBA	15792	10 degrees	3.97E-04
	3DSEM++	16219	10 degrees	**7.33E-05**
	ADBA	15128	20 degrees	8.01E-03
	ASDBA	15128	20 degrees	5.46E-03
	3DSEM++	15307	20 degrees	**6.53E-04**
Guitar String	ADBA	10819	4 degrees	8.29E-03
	ASDBA	10819	4 degrees	7.31E-03
	3DSEM++	11417	4 degrees	**2.24E-04**
	ADBA	10623	8 degrees	3.97E-03
	ASDBA	10623	8 degrees	1.49E-03
	3DSEM++	11175	8 degrees	**2.41E-04**
TEM *copper grid* bar	ADBA	6844	11 degrees	8.14E-04
	ASDBA	6844	11 degrees	5.63E-04
	3DSEM++	6941	11 degrees	**1.94E-05**
	ADBA	5726	22 degrees	1.06E-03
	ASDBA	5726	22 degrees	6.17E-04
	3DSEM++	5806	22 degrees	**8.22E-05**

Table 3.4: The accuracy results on a dataset including 167241 feature points from 2D SEM images. We used 80% of the dataset to train a prediction model, and 20% to test it. The accuracy, precision, and recall have been calculated using the equations 3.17 to 3.19.

Classifier	Accuracy	Precision	Recall
Naive Bayes	86.54%	87.91%	86.22%
SVM	93.07%	94.33%	91.79%
Random Forest	89.36%	91.04%	91.13%
Logistic Regression	83.26%	83.93%	82.44%

we used "Transom:Rotate Camera" filter to rotate a 3D face model artificially, and then took a photo from the face model. Fig. 3.11 shows how we generated 2D images from 3D face models in Meshlab. A sample 3D visualization example of a face model using our proposed 3D surface reconstruction technique on synthetic face models [90] is shown in Fig. 3.12.

Here, we computed the geometric difference between the 3D "*Face*" models (the reference model and the one obtained by our proposed system) using Hausdorff Distance unit (HDu) [28], [85]. HDu was developed several years ago to measure how close two subsets of a metric space are to each other. HDu has been defined as the maximum distance of a set to the nearest point in the other set [98]. HDu from set A to set B is a maximin function, defined as follows:

$$h(A, B) = max_{a \in A}\{min_{b \in B}\{d(a, b)\}\} \tag{3.20}$$

where a and b are points of sets A and B respectively, and d(a, b) is any metric (e.g., Euclidian distance) between these points. Maximum, minimum, and mean of HDu values were estimated between the original 3D "*Face*" model as a reference, with one obtained using the proposed 3D SEM surface modeling approach. We employed Meshlab [2] as an advanced 3D mesh processing application to estimate the HDu values. The HDu values which are presented in Table 3.5 state clearly that the proposed strategy can produce more accurate 3D surface models than the two other techniques. We also

Table 3.5: Hausdorff Distance unit values on the synthetic "*Face*" Models [90]. In this table, our system is denoted as 3DSEM++.

Dataset	Method	3D points	HDu (min)	HDu (max)	HDu (mean)
Face instance #1	ADBA	9118	0.000000	0.413316	0.100449
	ASDBA	9118	0.000031	0.160500	0.031006
	3DSEM++	9307	0.000004	0.021194	**0.004218**
Face instance #2	ADBA	6144	0.000017	0.193803	0.071284
	ASDBA	6144	0.000000	0.070409	0.009106
	3DSEM++	6872	0.000000	0.006088	**0.001407**
Face instance #3	ADBA	9605	0.000000	0.730032	0.240019
	ASDBA	9605	0.000049	0.096155	0.010137
	3DSEM++	10041	0.000014	0.016031	**0.007151**
Face instance #4	ADBA	7107	0.000000	0.319071	0.084141
	ASDBA	7107	0.000000	0.117512	0.017703
	3DSEM++	7583	0.000000	0.010619	**0.002019**

used the "*Face*" model instances to examine 3D rotation calibration by synthetic data. In doing so, we utilized Meshlab [2] and four instances of the "*Face*" model, rotating 3D models by different angles around X, Y, and Z axes. The results obtained by these experiments are presented in Table 3.6.

3.9 What Have We Learned Experimentally?

There have been a number of conclusions we have reached through the experimental validations. We briefly introduce them as follows:

- The experimental validations showed that SEM micrographs are suitable for 3D SEM surface reconstruction using our proposed multi-view, optimized, adaptive, and intelligent approach.

- Comparing two other traditional methods, our proposed method has produced better results in both SEM extrinsic calibration and 3D SEM surface reconstruction.

- The number of correct corresponding points has a crucial impact on the quality of 3D surface models reconstructed by our proposed method.

- Not all SEM images are proper for 3D surface reconstruction using the proposed approach. The proposed approach does not suit for either complex microscopic

Table 3.6: Comparison of the proposed optimized, adaptive, and intelligent method with two other traditional strategies, namely ADBA and ASDBA using the synthetic data. We labeled our proposed method as 3DSEM++. The Face instance #1 tilted over X axis, the Face instance #2 titled over Y, The Face instance #3 tilted over Z axis axis, and the Face instance #4 tilted over X axis.

Image set	Method	Total Matches	Rotation angle	ΔR
Face instance #1	ADBA	3940	5 degrees	4.13E-02
	ASDBA	3940	5 degrees	3.72E-02
	3DSEM++	4188	5 degrees	**6.31E-04**
	ADBA	3837	10 degrees	2.85E-02
	ASDBA	3837	10 degrees	1.63E-02
	3DSEM++	4039	10 degrees	**5.29E-04**
Face instance #2	ADBA	3629	10 degrees	2.52E-02
	ASDBA	3629	10 degrees	2.11E-02
	3DSEM++	3711	10 degrees	**4.66E-04**
	ADBA	3581	15 degrees	4.47E-02
	ASDBA	3581	15 degrees	2.19E-02
	3DSEM++	3679	15 degrees	**3.73E-04**
Face instance #3	ADBA	3512	15 degrees	5.26E-02
	ASDBA	3512	15 degrees	7.19E-03
	3DSEM++	3604	15 degrees	**3.07E-04**
	ADBA	3477	20 degrees	1.11E-02
	ASDBA	3477	20 degrees	2.21E-03
	3DSEM++	3568	20 degrees	**4.19E-04**
Face instance #4	ADBA	3312	25 degrees	3.14E-04
	ASDBA	3312	25 degrees	2.19E-04
	3DSEM++	3459	25 degrees	**2.90E-04**
	ADBA	3270	30 degrees	4.79E-03
	ASDBA	3270	30 degrees	3.21E-03
	3DSEM++	3366	30 degrees	**4.39E-04**

surfaces with shaded or very dark areas, or flat surfaces. In other words, the surface should contain trackable features.

- 3D rotation calibration using the synthetic data produced better promising results than real SEM images. This indicates that the 3D rotation angles provided by the SEM are not completely and exactly accurate.

- Larger rotation angles have positive impact on the rotation calibration as well as on the quality of 3D reconstructed surfaces. SEM micrographs taken at least every 9 or 10 degrees are recommended to produce a 3D surface model. Small rotation angles do not appear to be appropriate to restore a reliable 3D surface from 2D images.

- Microscopic samples must remain static during the SEM imaging process without any non-rigid deformation.
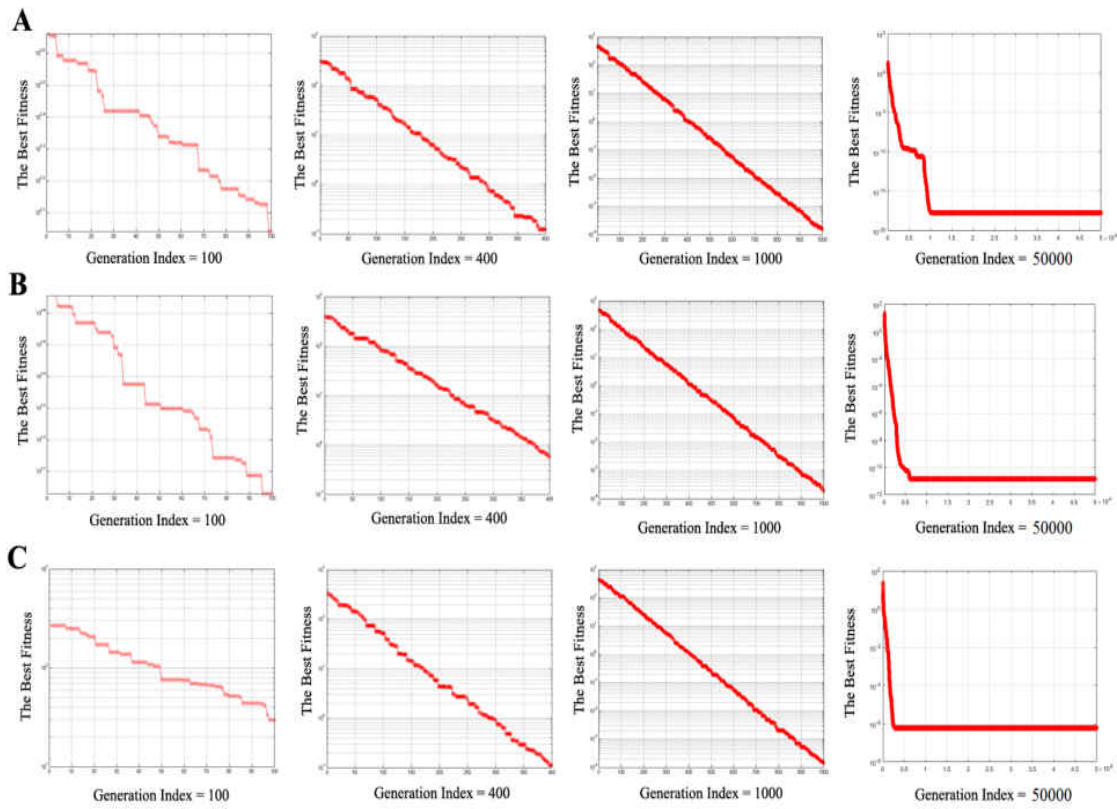
Figure 3.9: The convergence rates for *Pollen grain* (first row), TEM *copper grid* (second row), and *tapetal cell* (last row) with respect to different number of generations in Algorithm 2.1. Horizontal and vertical axes show the generation indexes, and the best fitnesses respectively.
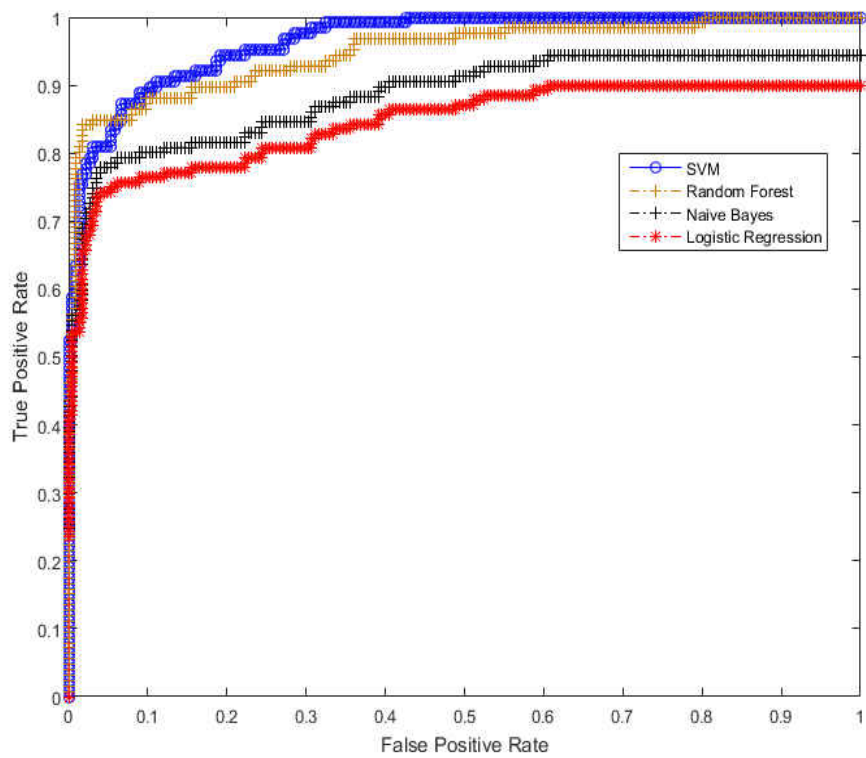
Figure 3.10: The ROC curve for the feature point dataset dataset shows that the area under the SVM classifier represents a better result compared to three other classification algorithms.
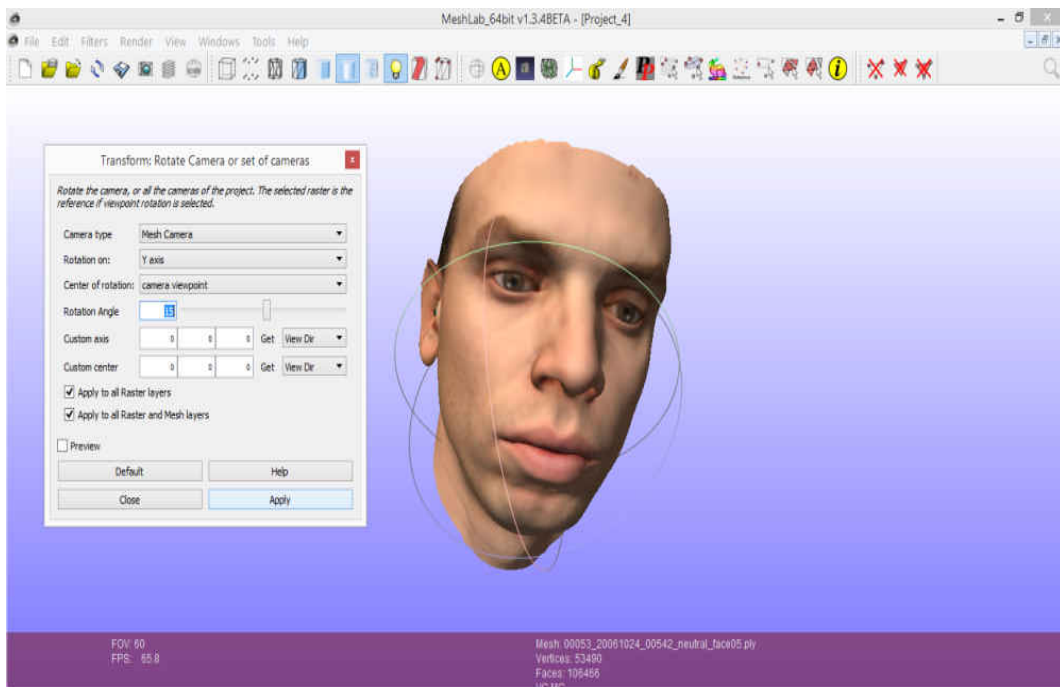
Figure 3.11: We utilized Meshlab to generate 2D images from the synthetic face models. We first load a 3D face model into Meshlab, then use "Transform:Rotate Camera" filter from the "Filter" menu. Using the "Rotation On" we can define the rotation axis. As you see in this figure, the rotation angle has been defined as 15 degrees and the rotation axis is around y.
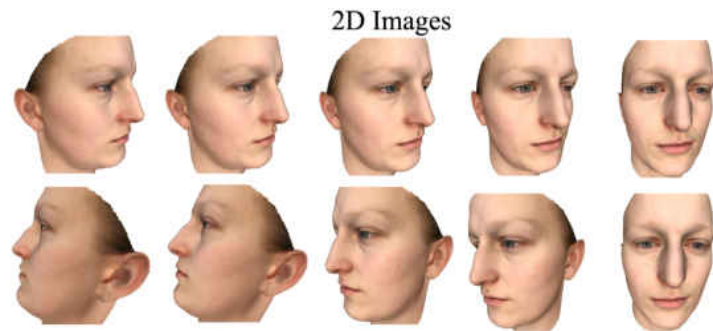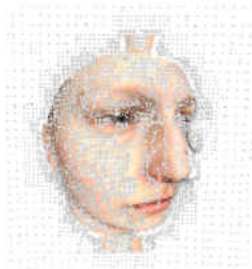
Figure 3.12: Quantitative validation and comparison of the proposed 3D SEM surface reconstruction. A set of 10 2D images of a synthetic "*Face*" model along with its 3D surface mesh and the reference structure are shown in this figure. The pose variations are -60, -40, -20, -10, -5, 0, 20, 35, 60, 65 degrees around Y-axis. 6872 3D points were used in the experiment to compare the accuracy on 3D shape modeling. Comparison of HDu value results for the model is presented in Table 3.5.

Chapter 4

The Dataset and Service Library

As a part of our contributions, in this chapter we will introduce a 3D SEM surface reconstruction dataset namely "3DSEM", and a service library called "SeLibCV" to advance the 3D SEM surface reconstruction research. We will first discuss the dataset, and then present the service library.

4.1 3DSEM: A 3D SEM Surface Reconstruction Dataset

The Scanning Electron Microscope (SEM) as a 2D imaging instrument has been widely used in many scientific disciplines including biological, mechanical, and materials sciences to determine the surface attributes of microscopic objects. However, the SEM micrographs still remain 2D images. To effectively measure and visualize the surface properties, we need to truly restore the 3D shape model from 2D SEM images. Having 3D surfaces would provide the anatomic shape of micro samples which would allow for quantitative measurements and informative visualization of the specimens being investigated. The 3DSEM is a dataset for 3D microscopy vision which is freely available at [5] for any academic, educational, and research purposes. The dataset includes both 2D images and 3D reconstructed surfaces of different real samples.

4.1.1 How the Data Was Acquired

2D SEM images were captured with a Hitachi S-4800 field emission scanning electron microscope (SEM). The 3D Shape models are created using the 3D SEM surface reconstruction algorithm illustrated in chapter 2. The models and the underlying technologies are fully explained in Chapter 2. The raw image data including 2D SEM images (SEM micrographs) are provided by the Departmen of Biological Sciences Electron Microscope

Table 4.1: Dataset Specifications.

Subject area	Microscopy Vision, Biology, Materials Sciences
Type of data	2D SEM Images (.JPEG, .TIFF), 3D Surface Models (.PLY, .OFF)
Data format	Digital Images, 3D Shape Models
Dataset location	University of Wisconsin-Milwaukee

Laboratory at University of Wisconsin-Milwaukee, USA. The 3D surface models including 3D point clouds (.ply format) and 3D surfaces (.off format) are provided by the Biomedical Modeling and Visualization Laboratory in the Computer Science Department at University of Wisconsin-Milwaukee, USA.

4.1.2 Value of the Dataset

- Discovering 3D surface structure from SEM images would provide anatomic surfaces and allow informative visualization of the objects being investigated.

- To provide the current dataset, an optimized, adaptive, and intelligent multi-view 3D SEM surface reconstruction algorithm is designed (Chapter 2).

- Several experimental validations are performed on real microscopic samples as well as synthetic data. The quantitative and qualitative results are promising (Chapter 3).

- Many research and educational questions truly require knowledge and information about 3D microscopic structures. The present dataset along with the algorithm would be helpful in this way.

- The current dataset, which includes 2D SEM images and 3D surface models, and the underlying methodology may serve as a guide for 3D SEM surface reconstruction.

4.1.3 Terms of Usage

The dataset is freely available for any academic, educational, and research purposes. The terms of usage include:

- 1) Users agree to cite [114] and [115] if the data is used for published research.

- 2) Users agree to use the data only for academic education or academic research.

- 3) Users agree to not distribute the data.

- 4) Users agree that the data may not be modified or used for non-academic purposes without prior approval.

4.2   SeLibCV: A Service Library to Advance 3D SEM Surface Reconstruction Research

Most of the underlying algorithms in 3D SEM surface reconstruction are complicated in code, and their implementations are available for only a few special platforms. This operational restriction causes various difficulties to utilize them, and even more, it makes different challenges to establish novel experiments and develop new research ideas. These computer vision strategies are essential for almost every computer vision problem, but their implementations are often available in binary (executable) format. Unavailability of multi platform implementations for such computer vision algorithms causes operational restrictions to examine new experiments and develop modern applications especially in the Internet of Things (IoT) era. SeLibCV is a Software as a Service (SaaS) library for computer vision and microscopy researchers worldwide that facilitates Rapid Application Development (RAD), and provides application-to-application interaction by tiny services accessible through the Internet. Its functionality covers a range of 3D SEM surface reconstruction algorithms including features detection and description, points matching, and 3D surface reconstruction and visualization. SeLibCV [111] is freely and publicly available at [6] for any academic, educational, and research purposes.

Concerning the software engineering, "Software as a Service" (SaaS) [9], [55] as the basic idea behind the centralized computing, is a design pattern as well as a delivery model in which a software could be accessed by human users through a web browser or by an application using an application-oriented interface [1], [9], [55]. To our best

knowledge, a SaaS based architecture has not yet been explored for highly demanded 3D SEM surface reconstruction algorithms and our work is one of the first to design and develop a set of World Wide Web services for the computer vision and microscopy community.

This contribution will target the following objectives: (1) To assist fast prototyping and Rapid Application Development (RAD) for the computer vision community by tiny services available on the Internet, (2) To provide application-to-application interaction for highly demanded 3D SEM surface reconstruction algorithms, (3) To make the fundamental 3D SEM surface reconstruction algorithms available through both human-oriented and application-oriented interfaces, (4) To provide better scalability in which the SeLibCV can spread all requests between different parallel data sources without having details of the resource to be implemented by service requesters, and (5) To create better portability and interoperability by imposing no programming language or operating system limitations in using the services.

Based on the unique architecture of SaaS [9], [55] and its functional attributes, it has a remarkable impact on the computer vision community by either bringing a modern architectural model which is distinguished from traditional software architectures, or allowing application-to-application communication through World Wide Web services. Employing SaaS architecture for computer vision algorithms will provide the following quality attributes: 1) Accessibility and availability, anywhere, anytime, 2) Interoperability, 3) Portability, 4) Less deployment time, and 5) Scalability.

The main idea of the work is that the SeLibCV could be considered as an initial step towards the next generation of computer vision applications.

4.2.1 System Architecture

The "4+1" view model [14], [44] as the most commonly used software architectural model template describes the anatomy of a software system using multiple concurrent views including Use Case view, Logical view, Process view, Development view, and Physical view. Here, we use the "4+1" view model to present and explain the Use Case and
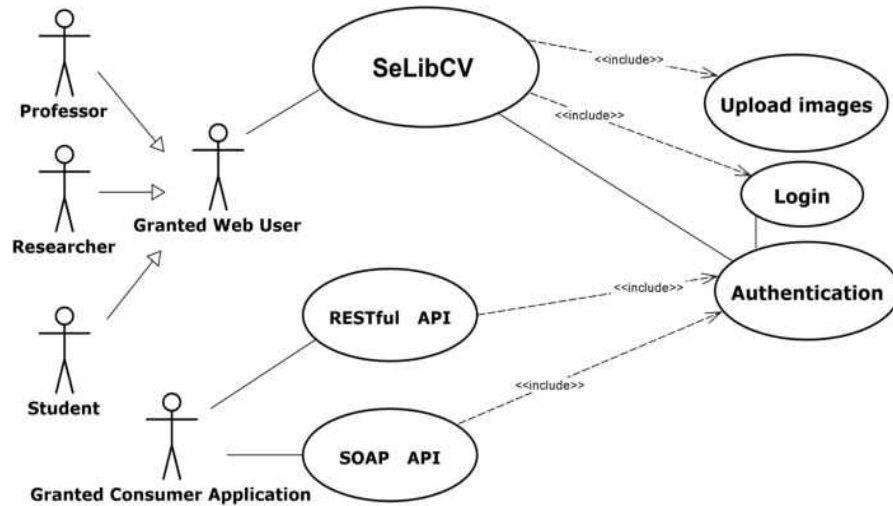
Figure 4.1: SeLibCV: Use Case View. This figure shows the main functionalities of the system and how different users can interact with those functionalities.

Process diagrams of the proposed system.

Use Case View: This view is one of the fundamental perspectives of the "4+1" view model which represents the main functionalities of the system along with their users who can interact with the system [14]. The Use Case view of the SeLibCV is shown in Fig. 4.1. Different users can login into the system as a previously granted user, and then they can utilize the SeLibCV through the web. In case they intend to use the web based functionalities, they have to upload their own images. The other option is that the SeLibCV services may be called as a RESTful or SOAP based API [106] for a granted consumer application developed with any programming language. In this case, the services will work on the local images which are located in the consumer application's machine.

Process View: The process view deals with the dynamic aspects of a system to show how objects will integrate into the the complete system based on a time sequence [14]. The sequence diagram of the process view is presented in Fig. 4.2.

4.2.2 Service Architecture

The high level service architecture of the SeLibCV is shown in Fig. 4.3. The service compromises two disparate machines: a service consumer (Client) and the service provider

64
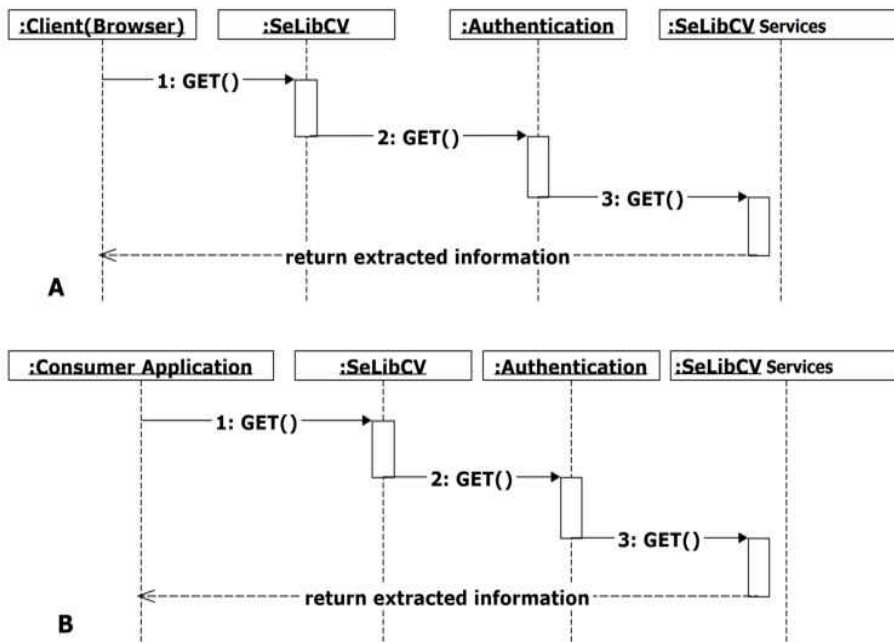
Figure 4.2: SeLibCV: Process View. The sequence diagram models the collaboration of objects based on a time sequence. GET() defines a particular communication between lifelines of an interaction. (A) A client by using an Internet browser can get into the system once after authentication. (B) A consumer application can also use the system once after authentication.
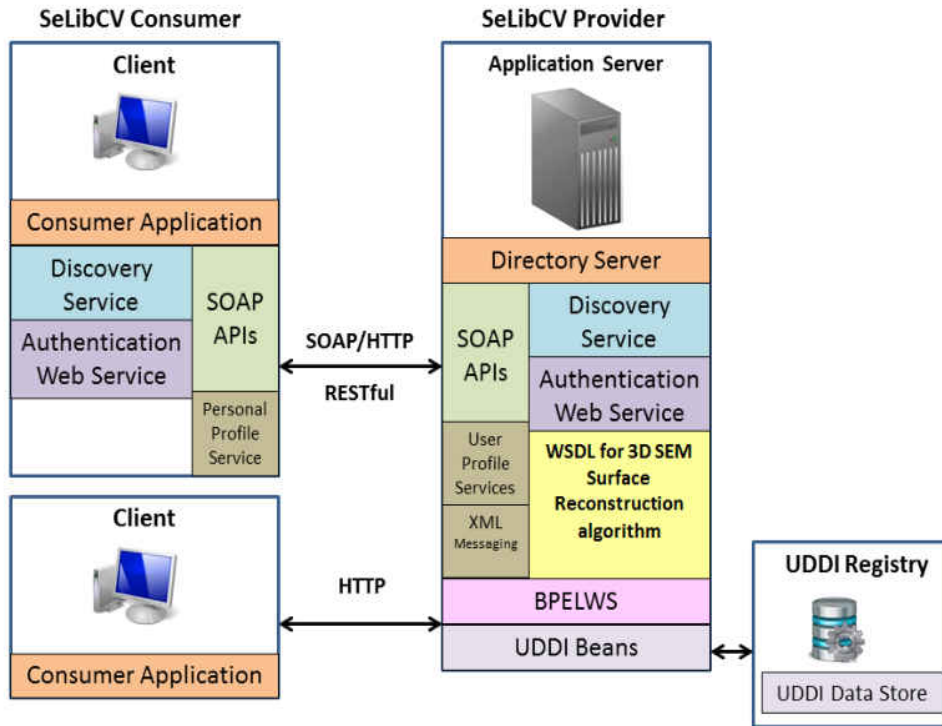
Figure 4.3: SeLibCV: Service architecture. WSDL (Web Service Description Language) is such an XML-based document for describing the SeLibCV services and how to access it over the standard Internet protocols. UDDI is a specification for a distributed type registry of the SeLibCV services which can communicate through SOAP, or Java RMI Protocols. Discovery Service permits the discovery of the SeLibCV services. SOAP (Simple Object Access Protocol) is a XML-based Internet protocol for exchanging structural information in the implementation of web services between computers and applications. BPELWS (Business Process Execution Language for Web Service) aims to model the main behaviors and operation of both executable and abstract implementation of the web service processes.

(Application Server). Main components of each section are presented within the subsystem blocks. The abstract view of the system is also shown in Fig. 4.4.

4.2.3   How to Use The SeLibCV Services

A complete user manual of the system is fully documented and available at [6]. In order to use the SeLibCV services, users should send a request for a valid username/password through [6]. We will then create and send them back the username/password to use the SeLibCV services either through an Internet browser or a consumer application. Using a

66
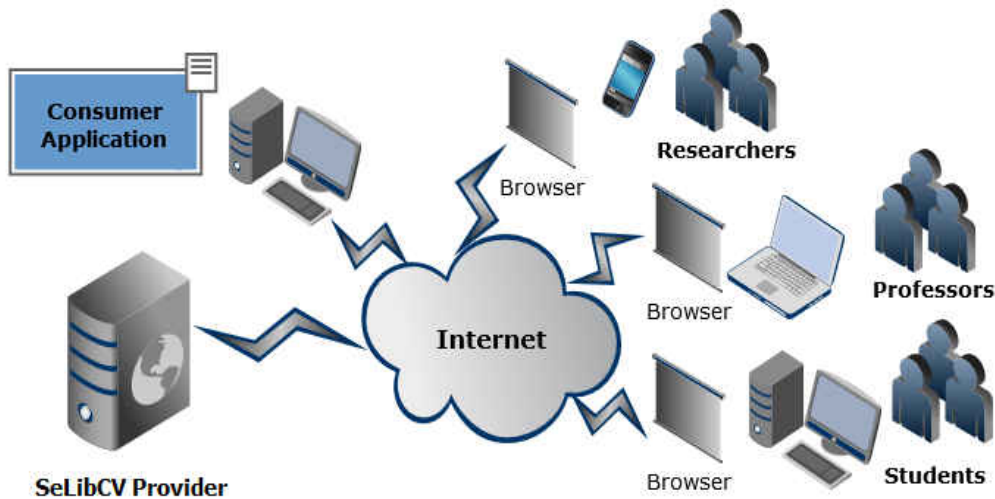
Figure 4.4: SeLibCV: Abstract view of the system. Different group of users can get into the system using a browser, and developers may build a consumer application to call the SeLibCV services without employing any browsers.

consumer application, the following sample code (Sample Code 4.1) is all that is necessary to call the SIFT algorithm inside the SeLibCV. This sample code is written in Java to get the SIFT description vectors.

SeLibCV is an ongoing research project being developed by the Biomedical Modeling and Visualization Laboratory in the Computer Science Department at University of Wisconsin-Milwaukee, USA. It is publicly and freely available for any academic, educational, and research purposes. Users may include scientist, students, professors, researchers, and Application Developers.

Sample Code 4.1. How to call the SIFT algorithm implemented in SeLibCV:

```
try {
    SiftResult sift = proxy.sift(USER, PASS, fileContent);
    BufferedImage img =
    ImageIO.read(new ByteArrayInputStream(sift.getImageDate()));
    ImageUtil.saveAsPNG(img, args[1]);
    System.out.println("Results SIFT Image saved as: "+ args[1]);
    System.out.println("SIFT result:");
    for(int i=0; i< sift.getPoints().length(); i++) {
```

```
        System.out.println("X: " + sift.getPoints[i].getX()+

    "Y: " + sift.getPoints[i].getY());}

    } catch (Exception e) {

        e.printStackTrace();

}
```

Chapter 5

Tribological Study in Micro Scale: An Application of 3D SEM Surface Reconstruction

Tribology [41] as a branch of materials and mechanical engineering sciences incorporates concepts of friction [82], wear [64], and lubrication to discover knowledge and facts about different surfaces. The SEM and the optical microscope (OM) are two common types of imaging equipment that have been used in tribological research to visualize and characterize worn surfaces. SEMs are more practical than the OMs since: 1) They are able to generate higher resolution and increased magnification as compared to OMs, and 2) They can also provide a greater depth of field. While SEM micrographs still remain two-dimensional (2D), tribological studies truly require information about three-dimensional (3D) surface structures. 3D surface reconstruction of SEM images is very widely used in the literature since it helps to analyze the surface roughness of worn surfaces [51] which can imply the wear and friction behavior of materials. In this chapter, copper pins were tested with a pin-on-disk tribometer on three different counterfaces (aluminum as softer material, copper with the same hardness, and stainless steel as harder material) and worn surfaces were further characterized by the proposed multi-view 3D SEM surface reconstruction approach. The surface roughness of pin is also calculated by using the 3D SEM surface reconstruction algorithm.

5.1 Sample Preparation

The dry pin-on-disk test (ASTM G99) was employed to investigate tribological behavior at room temperature. During the wear test, a stationary pin was forced into a rotating disk. Samples as pins were cut from as-received copper C110, with a contact surface of the rounded, 6mm diameter shape. The disks were of hardened 440C stainless steel

(harder than copper pin), C110 copper and aluminum 2024 (softer than copper pin). The sliding distance was fixed to 1 km, allowing the system to reach a steady friction and wear process. For each disk, at least three repetitive tests were performed. Subsequently the worn surfaces were examined by scanning electron microscope at different angles (0, 8, 15, 24 and 35 degrees). These images were used to reconstruct the 3D surface. SEM analysis was carried out on both etched and worn surfaces of specimens using a Hitachi S-4800 ultra high resolution cold cathode field emission scanning electron microscope (FE-SEM) operating at 10 kV.

5.2   3D Surface Roughness Measurement

After discovering the triangulated estimate of the surface model, the roughness of the surface between any given pair of points on the surface can be approximated. Assuming the two points of interest are called A and B, a line is drawn between the two points. Then, the line is projected onto the triangulated surface estimate. The 2D plot of the projected line represents the surface profile along AB direction. Then, the surface profile is rotated such that the starting and ending points are at the same height (line AB', Figure 5.1). The surface roughness is calculated as the average of the absolute value of the rotated surface profile:

$$R_a = \frac{1}{|AB|} \int_A^B |y(x)| dx$$
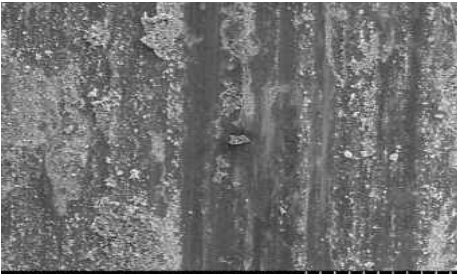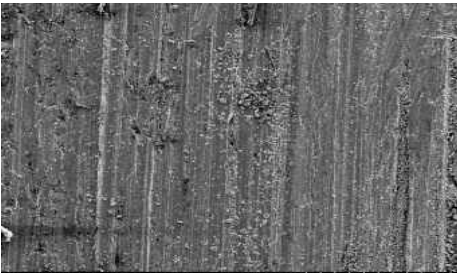
5.3   The Dataset

Dataset's names and attributes are shown in Table 5.1.

5.4   Tribological Analysis

The effects of the counterface materials on the dry-sliding coefficient of friction (COF) of the copper alloy are shown in Fig. 5.2. The average COF of copper alloy on aluminum, copper and stainless steel is 0.367, 0.540, and 0.268, respectively. The results of COF

Table 5.1: The Dataset Attributes.

Image sets	(1): An Aluminum Surface

(2): A Copper Surface

(3): A Stainless Steel Surface

Images properties	1280*960 grayscale, 512 dpi
Number of images in every set	5 SEM images
Rotation angle	0, 8, 15, 24 and 35 degrees
SEM detector	SE (mix)
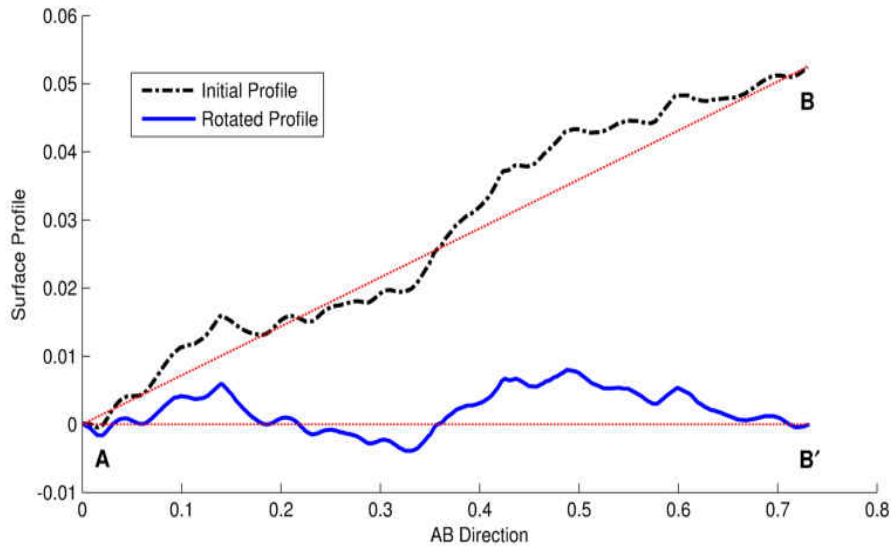
Figure 5.1: The surface profile between the two points A and B. Before finding the surface roughness, the profile is rotated such that line AB is horizontal.

exhibit that COF of copper alloy on stainless steel counterface is better than on the aluminum and copper counterface, and the steel counter face shows higher COF because of the formation of iron-rich layers that act as in-situ solid lubricants in the former case, but not on the surface of copper pins against copper and aluminum. The iron oxide rich layers are known to have low coefficient of friction. The linear wear-loss was acquired through a linear variable differential transducer (LVDT) with an encoder, which recorded the vertical displacement of the pin. Fig. 5.3 presents the amount of wear of the different mating disc pairs as a function of time. The results reveal that copper alloy has lower linear wear on stainless steel counterface while it shows higher linear wear on aluminum counterface due to formation of in-situ solid lubricants and decreasing the real contact area between copper pin and stainless steel disk. Another reason is that wearing the materials against a counterface which has a smaller thermal conductivity, led to the occurrence of severe wear. Therefore, wear of copper against aluminum and copper is higher than stainless steel counterface.

Fig. 5.4 shows the worn surface of pins used on different counterfaces. It is obvious that the wear rate of copper on an aluminum counterface is very high because of the visible large grooves and the large amount of debris on the surface of the copper, as shown in Fig. 5.4 (a). On the other hand, the surface of copper pins against copper and

72
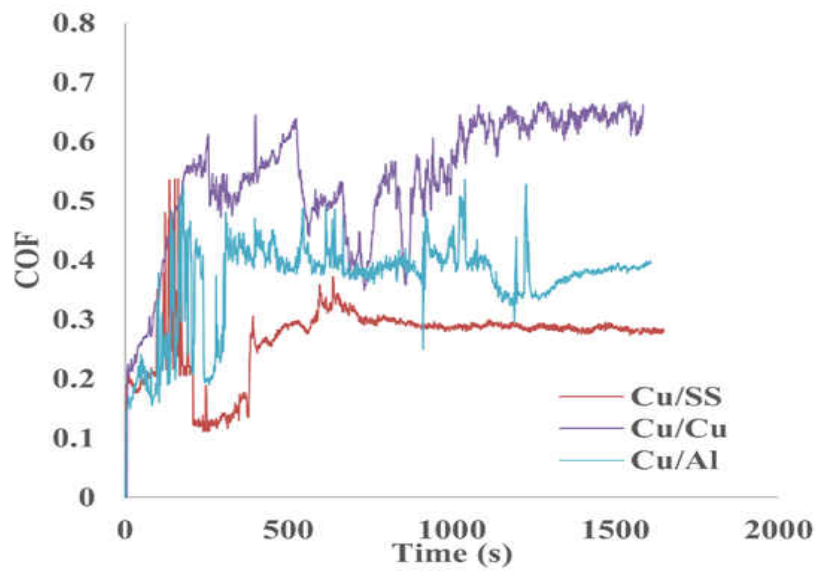
Figure 5.2: Variation of COF of copper pin against several counterfaces.
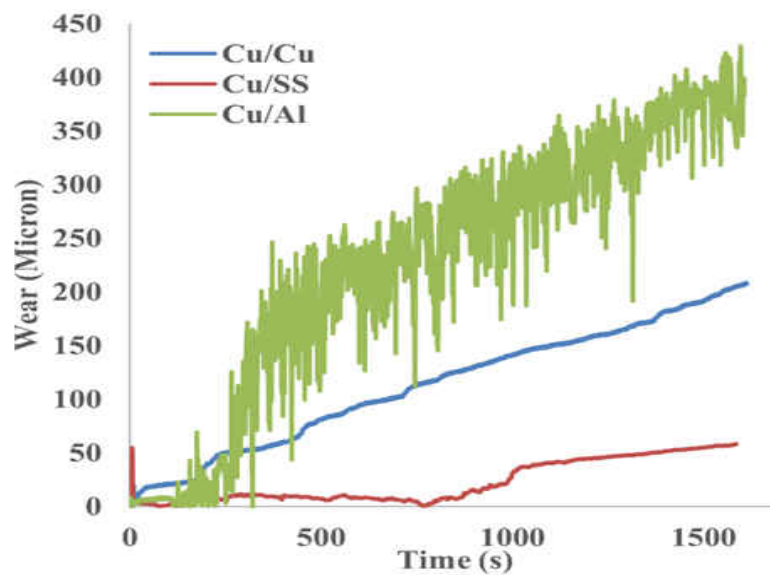
Figure 5.3: Variation of wear of copper pin against several counterfaces.
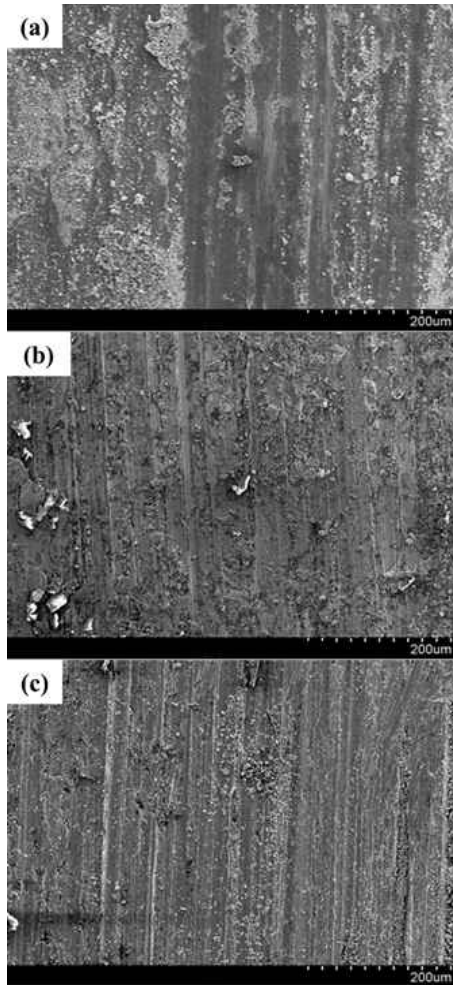
Figure 5.4: The SEM images of the worn surface of copper pins against a) aluminum, b) copper, and c) stainless steel.

stainless steel is smoother, and lower wear rate and less debris were observed on the worn surfaces. Fig. 5.5 shows the 3D topography image and linear topography of copper pin against different counterface. As expected, the worn surface of copper against aluminum is very rough, while smoother worn surfaces were observed for copper pins against copper and stainless steel disks.

Applications of the scanning electron microscope (SEM) in the material and mechanical sciences have contributed tremendously to our current understanding of surfaces at the micro level. SEM images can capture intricate details down to nm resolutions in the image plane. The problem is that the SEM images are initially limited to two-dimensional representations. 3D surface modeling of SEM images has progressively improved to allow the 3D characterization of different micro structures and surfaces.

74
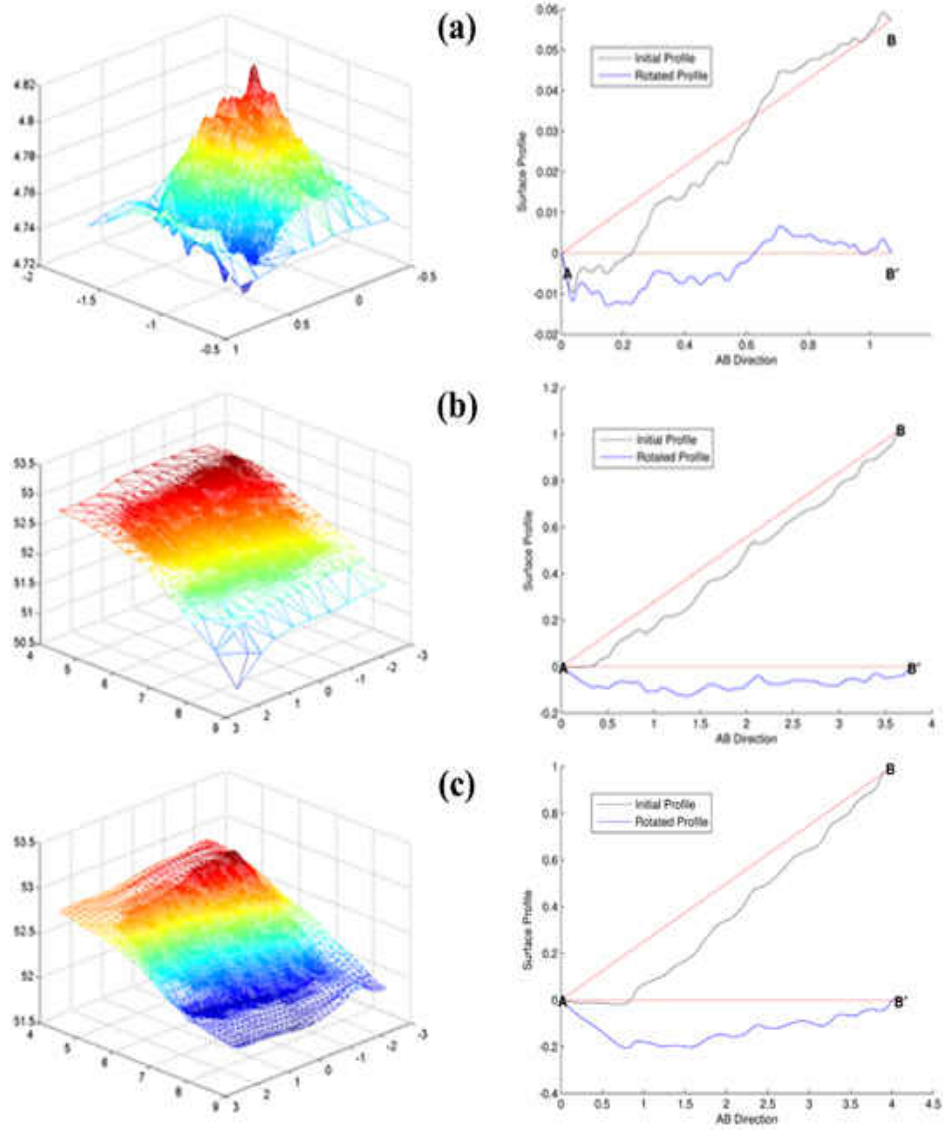
Figure 5.5: The 3D topography and linear topography of the worn surface of copper pins against a) aluminum, b) copper, and c) stainless steel.

In this research, a set of advanced computational algorithms have been combined to tackle the problem of tribological analysis at the micro scale. By taking advantage of the multiple view geometry and a global optimization method, we developed a 3D SEM surface reconstruction solution for the purpose of tribological analysis of micro surfaces. This study showed that 3D surface reconstruction of SEM images is well suited to tribological analysis of microscopic structures. The entire workflow does not need any specific computer hardware requirements, which makes it an inexpensive solution.

The quality of a resulting 3D surface model depends on various factors, such as surface structure, shape, the SEM micrograph quality and SEM imaging parameters. Complex surfaces as well as dark and shaded images are not suitable for the proposed algorithm.

This work opens up so many possibilities for seeing and examining micro surfaces in new ways that will certainly redefine the way we analyze the nanoworld samples. Improvements in such proposed 3D SEM surface reconstruction methods are necessary if the technique is to become fully integrated in materials sciences research.

Chapter 6

Conclusion and Outlook

The SEM, as one of the most highly used types of equipment in analyzing micro scale objects, employs electrons instead of light to determine the surface attributes of microscopic samples. The image formation in a SEM is based on the perspective projection in which the three dimensional object is projected onto a 2D image plane and, therefore, it contains no direct 3D information.

Having 3D surfaces from SEM images would assist analyzing true anatomic shapes of micro samples, providing quantitative measurements and informative visualization of the sample being investigated. To meet these requirements, this work focused on investigating adaptive and intelligent strategies to recover the 3D surface model of images acquired by a SEM. We integrated advanced computational technologies, such as machine learning, *a contrario* model estimation, and epipolar geometry to make an efficient multi-view 3D SEM surface reconstruction framework, namely 3DSEM++. A detailed performance evaluation and comparison of the proposed system with other traditional methods has also been carried out. The promising validation results of extensive experiments from different perspectives using both real microscopic samples as well as synthetic data are reported in this contribution.

This pilot study was leveraging computational methods for the purpose of 3D SEM surface modeling. The presented strategy is quite useful for the fast growing SEM application area and it is a remarkable extension for teaching purposes.

There are a number of outstanding issues with 3D SEM surface reconstruction techniques which we discuss here. We divide this section into two parts. In Section 6.1, we first point out the problems and challenges in SEM-based 3D surface reconstruction, and then, in Section 6.2, we address several insights and directions for possible future enhancements in this rapidly progressing field.

6.1 Problems and Challenges

In this section, we discuss the problems and challenges in 3D SEM surface reconstruction using different techniques as illustrated in the taxonomy (Fig. 1.2).

Invisible parts will not be reconstructed The main problem is that both single-view and multi-view 3D SEM surface reconstruction algorithms are applicable for those surfaces which are completely visible in a sample. Invisible and occluded parts by other objects or components will not be restored.

Distortions and noise in SEM images Like any other microscopic devices, the SEM images are vulnerable to different types of errors which interfere with a pure signal. The most prominent errors include: 1) Image distortions caused by the plane array of the detectors, 2) The elements of this array might have unequal sensitivity causing error, 3) Also, the quadruple detector system being asymmetric generates some errors, and 4) Noise as an unwanted component generated during the whole process of SEM imaging causes some errors as well [42].

Multiple highlights and shadows Employing BSE detectors, the SEM images will suffer from multiple highlights and shadowing effects. The presence of shadows or highlights have been responsible for reducing the reliability of 3D SEM surface reconstruction techniques, in particular for single-view approaches [11].

Limited number of images The other problem is that we may have to reconstruct the 3D surface model from a small number of SEM images. While the accuracy of multi-view 3D SEM surface reconstruction strategies needs a large number of images, the SEM specimen can tilt only from -5 to at most 70 degrees, depending on the size of the specimen mount (usually diameter) that the sample is mounted on as well as on the location of the specimen (Z or height) within the column of the microscope. These constraints limit the number of images that may be taken. On the other hand, small rotation angle does not appear to be appropriate to restore a reliable 3D surface from 2D images.

Vanishing points In multi-view 3D SEM surface reconstruction algorithms, one critical problem arises from vanishing points in the image sequence. Using multi-view

surface reconstruction systems, we use projective geometry principal to initialize the 3D position of only matching points in the image set. As we begin considering more than two images, it becomes unlikely that all matching points in the first image pair are observable in the other pairs. The only existing way to tackle the problem is using the incremental pipeline [68], [127]. The incremental multi-view 3D surface reconstruction is an iteratively growing reconstruction process in which it starts from an initial two-view reconstruction, and then is iteratively extended by adding new views and 3D points, using both pose estimation and triangulation. The technique was employed as part of our proposed method.

6.2 Possible Future Enhancements

Here, we point out different future enhancements which may affect the research in several ways.

Low-level and medium-level image processing techniques   In the previous section we mentioned several sources in the SEM which produce different kinds of noises, highlights and multiple shadows on SEM images, which consequently decrease the reliability and accuracy of 3D SEM surface modeling. Digital image processing techniques are widely used in such areas due to their ability to reduce noises [102], detect shadows [65] and highlights, and remove them from the original images. One future enhancement is to create a system that can automatically perform low and medium level image processing algorithms to provide better 2D images such that they can help us to produce much more reliable 3D surfaces.

Application area   The value of any research might be evaluated by how effective it is in real applications. We introduced several applications of the 3D SEM surface reconstruction in Chapter 1. A desirable improvement would be expanding the application areas from bioscience, material, and mechanical engineering to other scientific domains which need to know and evaluate the 3D shape information. The present work is expected to stimulate more interest and draw attention from the computer vision community to

the fast-growing SEM application area.

Public datasets   Recovering the structures of SEM images requires having a database which includes large number of different SEM images captured under wide variety of illumination directions as well as from different perspectives. We foresee a need to extend such a public and global database over the Internet to examine and analyze the 3D SEM Surface reconstruction methods by applying them to various microscopic samples and SEM images.

Dense Matching   Not every microscopic object is proper for 3D SEM surface reconstruction using our proposed model. The microscopic sample must remain static during the imaging process without any non-rigid deformations. The other limitation is that the proposed approach does not suit for either complex micro surfaces with very dark areas or flat surfaces. In other words, the surface should contain trackable features. The remedy can be sought in more elaborate matching methods by utilizing dense matching instead of sparse matching. In such techniques, the first step of the matching process, keypoint localization, is eliminated and descriptors are defined for every pixel in the image instead. By using such techniques, one can define smoothness constraints on the matching energy functional to account for featureless regions in the images.

Embedded system architecture community   As we discussed in Section 1, 3D SEM surface reconstruction showed a great success in a variety of applications. However, its extensive computational complexity has been a problem to implement such a real-time system. Considering hardware issues along with effective embedded system design [92], [132] will reduce the time complexity and should be able to provide real-time 3D microscopy vision.

Machine learning community   There is not yet a principal computation innovation based on the machine learning approaches. We believe that some novel solutions are beyond the scope of computer vision and require collaboration from the machine learning and artificial intelligence community. The resulting algorithms will allow researchers to achieve higher accuracy with limited computational complexity, and make the approaches appropriate for real-time operations.

Software architecture and Internet of Things community As an important enhancement, it is beneficial to design, develop and implement a set of web services, such as the reusable, platform independent, and extensible software components for 3D SEM vision to allow application-to-application interaction over the standard Internet protocols [56], [57], [128], [129]. These web services will provide a distributed platform to create communication between the highly demanding computer vision applications and World Wide Web services, and open the doors from the 3D microscopy vision to the Internet of Things (IoT) area [12], [70], [124].

Plug 3D SEM into the Cloud Cloud computing is one of the most discussed topics in the computer science world in recent years. Today, people choose cloud applications in cases where they have more integrity as well as low-cost implementations. On the other hand, several big software companies have started the development of cloud services to explore the benefits of incorporating such cloud architecture services in their own business. As the number of Cloud computing services are increasing rapidly, the essential need for such a particular framework appears. Plugging 3D SEM surface reconstruction into the Cloud would take full advantages of Cloud computing by deploying 3D microscopy vision as a service in private Clouds with Amazon or Google for vastly expanding research, academic and educational purposes.

Bibliography

[1] World wide web consortium. http://www.w3.org/.

[2] Meshlab. 2005. http://meshlab.sourceforge.net/.

[3] Mex software. 2005. Graz, Austria: Alicona Imaging GmbH.

[4] Weka 3: Data mining software in java. 2013. http://www.cs.waikato.ac.nz/ml/weka/.

[5] 3dsem. 2015. http://selibcv.org/3dsem.

[6] Selibcv. 2015. http://selibcv.org.

[7] S. Agarwal, Y. Furukawa, N. Snavely, I. Simon, B. Curless, S. M. Seitz, and R. Szeliski. Building rome in a day. *Commun. ACM*, 54(10):105–112, 2011.

[8] B. Albouy, S. Treuillet, Y. Lucas, and D. Birov. Fundamental matrix estimation revisited through a global 3d reconstruction framework. *in Advanced Concepts for Intelligent Vision Systems*, 2004.

[9] M. Almorsy, J. Grundy, and A. Ibrahim. Adaptable, model-driven security engineering for saas cloud-based applications. *Automated Software Engineering*, 21:187–224, 2014.

[10] N. S. Altman. An introduction to kernel and nearest-neighbor nonparametric regression. *The American Statistician*, 46:175–185, 1992.

[11] V. Argyriou and M. Petrou. Recursive photometric stereo when multiple shadows and highlights are presents. In *IEEE conference on Computer Vision and Pattern Recognition*, 2006.

[12] L. Atzori, A. Iera, and G. Morabito. Social internet of things: Turning smart objects into social objects to boost the iot. *Newsletter*, 2015, 2016.

[13] Z. Bardosi, D. Granata, G. Lugos, A. Tafti, and S. Saxena. Metacarpal bones localization in x-ray imagery using particle filter segmentation. *arXiv preprint arXiv:1412.8197*, 2014.

[14] L. Bass, P. Clements, and R. Kazman. *Software Architecture in Practice*. Addison-Wesley, 2013.

[15] H. Bay, A. Ess, T. Tuytelaars, and L. V. Gool. Surf: Speed up robust features. *Computer Vision and Image Understanding (CVIU)*, 110:346–359, 2008.

[16] H. Bay, T. Tuytelaars, and L. V. Gool. Speeded up robust features. In *European Conference of Computer Vision (ECCV)*, Graz, Austria, 2006.

[17] A. Ben-Hur, D. Horn, H. T. Siegelmann, and V. Vapnik. Support vector clustering. *The Journal of Machine Learning Research*, 2:125–137, 2002.

[18] A. Bogner, P. H. Jouneau, G. Thollet, D. Basset, and C. Gauthier. A history of scanning electron microscopy developments: towards wet-stem imaging. *Micron*, 38:390–401, 2007.

[19] J. J. Bozzola and L. D. Russel. *Electron Microscopy*. Jones and Bartlett, USA, 1992.

[20] J. J. Bozzola and L. D. Russell. *Electron microscopy: principles and techniques for biologists*. Jones & Bartlett Learning, 1999.

[21] L. Breiman. Random forests. *Machine learning*, 45(1):5–32, 2001.

[22] M. Calonder, V. Lepetit, C. Strecha, and P. Fua. Brief: Binary robust independent elementary features. In *Springer ECCV*, 2010.

[23] L. Carli, G. Genta, A. Cantatore, G. Barbato, L. D. Chiffre, and R. Levi. Uncertainty evaluation for three-dimensional scanning electron microscope reconstructions based on the stereo-pair technique. *Measurement Science and Technology*, 22(3):035103, 2011.

[24] J. Cazaux. Recent developments and new strategies in scanning electron microscopy. *Journal of Microscopy*, 217:16–35, 2005.

[25] U. K. Chakraborty. *Advances in Differential Evolution*. Prentice Hall, USA, 2008.

[26] D. E. Chandler and R. W. Robertson. *Bioimaging: current concepts in light and electron microscopy*. Jones and Bartlett, USA, 2009.

[27] D. Chen, A. Miyamoto, and S. Kaneko. Robust surface reconstruction in sem with two bse detectors. *Mecatronics REM 2012*, 2012.

[28] P. Cignoni, C. Rocchini, and R. Scopigno. Metro: Measuring error on simplified surfaces. *Computer Graphics Forum*, 17:167–174, 1998.

[29] N. Cornille, D. Garcia, M. Sutton, and S. McNeill. Automated 3d reconstruction using a scanning electron microscope. In *SEM Annual Conference and Exposition on Experimental and Applied Mechanics*, 2003.

[30] C. Cortes and V. Vapnik. Support-vector networks. *Machine learning*, 20(3):273–297, 1995.

[31] D. R. Cox. The regression analysis of binary sequences. *Journal of the Royal Statistical Society. Series B (Methodological)*, pages 215–242, 1958.

[32] D. Crandall, A. Owens, N. Snavely, and D. Huttenlocher. Discrete-continuous optimization for large-scale structure from motion. In *CVPR 2011*, 2011.

[33] B. Cyganek and J. P. Siebert. *An Introduction to 3D computer vision techniques and algorithms*. Wiley, UK, 2009.

[34] R. Danzl and S. Scherer. Integrating shape from shading and shape from stereo for variable reflectance surface reconstruction from sem images. In *SEM Images, 26th Workshop of the Austrian Association for Pattern Recognition*, 2003.

[35] S. Das, S. S. Mullick, and P. Suganthan. Recent advances in differential evolution– an updated survey. *Swarm and Evolutionary Computation*, 27:1–30, 2016.

[36] J. C. Davis and R. J. Sampson. *Statistics and data analysis in geology*, volume 646. Wiley New York et al., 1986.

[37] A. Desolneux, L. Moisan, and J.-M. Morel. Meaningful alignments. *International Journal of Computer Vision*, 40(1):7–23, 2000.

[38] A. Desolneux, L. Moisan, and J.-M. Morel. Meaningful alignments. *International Journal of Computer Vision*, 40(1):7–23, 2000.

[39] A. Desolneux, L. Moisan, and J.-M. Morel. *From gestalt theory to image analysis: a probabilistic approach*, volume 34. Springer Science & Business Media, 2007.

[40] A. Desolneux, L. Moisan, and J.-M. Morel. *From gestalt theory to image analysis: a probabilistic approach*, volume 34. Springer Science & Business Media, 2007.

[41] D. Dowson. *History of tribology*. Addison-Wesley Longman Limited, 1979.

[42] W. Drzazga, J. Paluszynski, and W. Slowko. Three-dimensional characterization of microstructures in a sem. *Measurement Science and Technology*, 17:28–31, 2006.

[43] R. Egerton. *Physical Principles of Electron Microscopy: An Introduction to TEM, SEM, and AEM*. Springer, USA, 2005.

[44] H.-E. Eriksson and M. Penker. *Business modeling with UML*. John Wiley and Sons, 2000.

[45] V. Estellers, J.-P. Thiran, and M. Gabrani. Surface reconstruction from microscopic images in optical lithography. *IEEE Transactions on Image Processing*, 23(8):3560–3573, 2014.

[46] V. Feoktistov. *Differential Evolution*. Springer, Germany, 2006.

[47] M. A. Fischler and R. C. Bolles. Random sample consesus: a paradigm for model fitting with applications to image analysis and automated cartography. In *Communications of the ACM*, 1981.

[48] S. L. Flegler, J. W. Heckman, K. L. Klomparens, K. L. Klomparens, and K. L. Klomparens. *Scanning and transmission electron microscopy: an introduction.* WH Freeman New York, 1993.

[49] D. A. Freedman. *Statistical models: theory and practice.* cambridge university press, 2009.

[50] K. Fridman, A. Mader, M. Zwerger, N. Elia, and O. Medalia. Advances in tomography: probing the molecular architecture of cells. *Nat Rev Mol Cell Bio*, pages 736–742, 2012.

[51] E. Gadelmawla, M. Koura, T. Maksoud, I. Elewa, and H. Soliman. Roughness parameters. *Journal of Materials Processing Technology*, 123(1):133–145, 2002.

[52] A. Ghosh, A. Mondal, and S. Ghosh. Moving object detection using markov random field and distributed differential evolution. *Applied Soft Computing*, 15:121–136, 2014.

[53] M. Hall, E. Frank, G. Holmes, B. Pfahringer, P. Reutemann, and I. H. Witten. The weka data mining software: an update. *ACM SIGKDD explorations newsletter*, 11(1):10–18, 2009.

[54] R. Hartely and A. Zisserman. *Multiple view geometry in computer vision.* Cambridge University Pressy, UK, 2004.

[55] R. Hatch. *SaaS Architecture, Adoption and Monetization of SaaS Projects using Best Practice Service Strategy, Service Design, Service Transition, Service Operation and Continual Service Improvement Processes.* Emereo Pty Ltd, 2008.

[56] R. Hatch. *SaaS Architecture, Adoption and Monetization of SaaS Projects using Best Practice Service Strategy, Service Design, Service Transition, Service Operation and Continual Service Improvement Processes.* Emereo Pty Ltd, 2008.

[57] R. Hatch. *SaaS Architecture, Adoption and Monetization of SaaS Projects using*

Best Practice Service Strategy, Service Design, Service Transition, Service Operation and Continual Service Improvement Processes. Emereo Pty Ltd, 2008.

[58] H. Hayakawa. Photometric stereo under a light source with arbitrary motion. *Journal of the Optical Society of America*, pages 3079–3089, 1994.

[59] T. K. Ho. Random decision forests. In *Document Analysis and Recognition, 1995., Proceedings of the Third International Conference on*, volume 1, pages 278–282. IEEE, 1995.

[60] L. G. Hobrough. Methods and apparatus for correlating corresponding points in two images. (US67997857A), 1957.

[61] B. K. P. Horn. Shape from shading: a method for obtaining the shape of a smooth opaque object from one view. *MIT, Technical Report*, 1970.

[62] K. Ikeuchi and B. K. P. Horn. *Numerical shape from shading and occluding boundaries.* 1981.

[63] M. Kantardzic. *Data mining: concepts, models, methods, and algorithms.* John Wiley & Sons, 2011.

[64] K. Kato and K. Adachi. Wear mechanisms. *Modern tribology handbook*, 1:273–300, 2001.

[65] D. Kersten, P. Mamassian, and D. C. Knill. Moving cast shadows induce apparent motion in depth. *Perception*, 26:171–192, 1997.

[66] S. Kirkpatrick, C. D. Gelatt, and M. P. Vecchi. Optimization by simulated annealing. *Science*, 220:671–680, 1983.

[67] C. Kizilyaprak, J. Daraspe, and B. M. Humbel. Focused ion beam scanning electron microscopy in biology. *J Microsc*, pages 109–114, 2014.

[68] M. Klopschitz, A. Irschara, G. Reitmayr, and D. Schmalstieg. Robust incremental structure from motion. In *Fifth International Symposium on 3D Data Processing, Visualization and Transmission (3DPVT)*, 2010.

[69] T. Kodama, X. Li, K. Nakahira, and D. Ito. Evolutionary computation applied to the reconstruction of 3-d surface topography in the sem. *Journal of Electron Microscopy*, 54(5):429–435, 2005.

[70] H. Kopetz. Internet of things. In *Real-time systems*, pages 307–323. Springer, 2011.

[71] R. Kozera, T. Cameron, and A. Datta. A parallel leap-frog algorithm for 3-source photometric stereo. In *Computational Imaging and Vision, ICCVG'04*, 2006.

[72] R. Kozera and L. Noakes. A 2d lead-frog algorithm for optimal surface reconstruction. In *proc SPIE99, Vision Geometry VIII-3811*, 1999.

[73] N. Lazaros, G. C. Sirakoulis, and A. Gasteratos. Review of stereo vision algorithms: From software to hardware. *International Journal of Optomechatronics*, 2:435–462, 2008.

[74] Y. Li, N. Snavely, D. Huttenlocher, and P. Fua. Worldwide pose estimation using 3d point clouds. In *ECCV*, 2012.

[75] X. Liu, H. Hu, W. Jiang, and X. Sun. Object-oriented modified photometric stereo algorithm for 3d imaging in fiber-to-chip coupling. In *IEEE 9th international conference on Group IV Photonics (GFP)*, 2012.

[76] H. Longuet-Higgins. A computer algorithm for reconstructing a scene from two projections. *Nature*, 293(10):133–135, 1981.

[77] M. A. Lourakis and A. Argyros. Sba: A software package for generic sparse bundle adjustment. *ACM Trans. Math. Software*, 36(1):1–30, 2009.

[78] D. G. Lowe. Distinctive image features from scale-invariant keypoints. *International Journal of Computer Vision*, 60(2):91–110, 2004.

[79] K. V. Mardia. *Statistics of directional data*. Academic Press, 2014.

[80] F. Marinello, P. Bariani, E. Savio, A. Horsewell, and L. D. Chiffre. Critical factors in sem 3d stereo microscopy. *Measurement Science and Technology*, 19(6):065705, 2008.

[81] A. McCallum, K. Nigam, et al. A comparison of event models for naive bayes text classification. In *AAAI-98 workshop on learning for text categorization*, volume 752, pages 41–48. Citeseer, 1998.

[82] P. L. Menezes, M. Nosonovsky, S. V. Kailas, and M. R. Lovell. Friction and wear. In *Tribology for Scientists and Engineers*, pages 43–91. Springer, 2013.

[83] T. M. Mitchell. Machine learning., 1997.

[84] J. L. Mundy, A. Zisserman, et al. *Geometric invariance in computer vision*, volume 92. MIT press Cambridge, MA, 1992.

[85] Munkres and James. *Topologyn.* Prentice Hall, USA, 1999.

[86] C. Nyirarugira and K. Taeyong. Adaptive differential evolution algorithm for real time object tracking. *IEEE Transaction on Consumer Electronics*, 59, 2013.

[87] A. Okabe, B. Boots, K. Sugihara, and S. N. Chiu. *Spatial Tessellations: concepts and applications of voronoi diagram.* Wiley, USA, 2000.

[88] J. Paluszynski and W. Slowko. Surface reconstruction with the photometric method in sem. *Vaccum*, 78:533–537, 2005.

[89] K. D. Parry-Vernon. Scanning electron microscopy: an introduction. *III-Vs Review*, 13:40–44, 2000.

[90] P. Paysan, R. Knothe, B. Amberg, S. Romdhani, and T. Vetter. A 3d face model for pose and illumination invariant face recognition. In *Proceedings of the 6th IEEE International Conference on Advanced Video and Signal based Surveillance (AVSS) for Security, Safety and Monitoring in Smart Environments*, Genova, Italy, 2009.

[91] R. Pintus, S. Podda, and M. Vanzi. An automatic alignment procedure for a 4-source photometric stereo technique applied to scanning electron microscopy. *IMTC- Instrumentation and Measurement*, pages 989–996, 2006.

[92] J. Qiu, T. Huang, and T. Ikenaga. A fpga-based dual-pixel processing pipelined hardware accelerator for feature point detection part in sift. *International Joint Conference on INC, IMS, and IDC*, pages 1668–1675, 2009.

[93] J. Rabin, J. Delon, and Y. Gousseau. A statistical approach to the matching of local features. 2009.

[94] M. Raspanti, E. Binaghi, I. Gallo, and A. Manelli. A vision-based 3d reconstruction techniques for scanning electron microscopy: Direct comparison with atomic force microscopy. *Microscopy Reserach and Techniques*, 67:1–7, 2005.

[95] I. Rish. An empirical study of the naive bayes classifier. In *IJCAI 2001 workshop on empirical methods in artificial intelligence*, volume 3, pages 41–46. IBM New York, 2001.

[96] J. Rittscher, R. Machiraju, and S. T. C. Wong. *Microscopic image analysis for life science and applications*. Artech House, USA, 2008.

[97] L. Roberts. Machine perception of three-dimensional solids. *MIT, PhD Thesis*, 1963.

[98] G. Rote. Computing the minimum hausdorff distance between two point sets on a line under translation. *Information Processing Letters*, 38(3):123–127, 1991.

[99] P. Rousseeuw. Least median of squares regression. *Journal of the American Statistical Association*, 79:871–880, 1984.

[100] E. Rublee. Orb: An efficient alternative to sift or surf. In *IEEE International Conference on Computer Vision*, 2011.

[101] D. Samak, A. Fischer, and D. Rittel. 3d reconstruction and visualization of microstructure surfaces from 2d images. *Annals of the CIRP*, 56:149–152, 2007.

[102] L. Shao, R. Yan, X. Li, and Y. Liu. From heuristic optimization to dictionary learning: a review and comprehensive comparison of image denoising algorithms. *IEEE Transactions on Cybernetics*, pages 1001–1013, 2014.

[103] J. Shotton, A. Fitzgibbon, M. Cook, T. Sharp, M. Finocchio, R. Moore, A. Kipman, and A. Blake. Real-time human pose recognition in parts from a single depth image. In *CVPR 2011*, 2011.

[104] W. Slowko and M. Krysztof. Detector system for three-dimensional imaging in the variable pressure/environmental sem. In *IX International conference ION*, 2013.

[105] N. Snavely, S. M. Seitz, and R. Szeliski. Modeling the world from internet photo collections. *International Journal of Computer Vision*, 80:189–210, 2008.

[106] L. Srinivasan and J. Treadwell. An overview of service-oriented architecture, web services, and grid computing. *HP Software Global Business Unit*, 2005.

[107] R. Storn. On the usage of differential evolution for function optimization. In *Fuzzy Information Processing Society, 1996. NAFIPS., 1996 Biennial Conference of the North American*, pages 519–523. IEEE, 1996.

[108] R. Storn and K. Price. *Differential evolution-a simple and efficient adaptive scheme for global optimization over continuous spaces*, volume 3. ICSI Berkeley, 1995.

[109] P. Sturm. Multi-view geometry for general camera models. In *Computer Vision and Pattern Recognition, 2005. CVPR 2005. IEEE Computer Society Conference on*, volume 1, pages 206–212. IEEE, 2005.

[110] A. P. Tafti, A. Baghaie, A. Kirkpatrick, H. Owen, R. DSouza, and Z. Yu. A comparative study on the application of sift, surf, brief and orb for 3d surface reconstruction of electron microscopy images. *Computer Methods in Biomechanics and Biomedical Engineering: Imaging & Visualization*, 2016.

[111] A. P. Tafti, H. Hassannia, D. Piziak, and Z. Yu. Selibcv: A service library for computer vision researchers. In *Advances in Visual Computing*, pages 542–553. Springer, 2015.

[112] A. P. Tafti, H. Hassannia, and Z. Yu. siftservice.com: Turning a computer vision algorithm into a world wide web service. *arXiv preprint arXiv:1504.02840*, 2015.

[113] A. P. Tafti, A. Kirkpatrick, H. Owen, and Z. Yu. 3d microscopy vision using multiple view geometry and differential evolutionary approaches. In *Advances in Visual Computing*, pages 141–152. Springer, 2014.

[114] A. P. Tafti, A. B. Kirkpatrick, Z. Alavi, H. A. Owen, and Z. Yu. Recent advances in 3d sem surface reconstruction. *Micron*, 78:54–66, 2015.

[115] A. P. Tafti, A. B. Kirkpatrick, J. D. Holz, H. A. Owen, and Z. Yu. 3dsem: A 3d microscopy dataset. *Data in Brief*, 6:112–116, 2016.

[116] C. Tomasi and T. Kanade. Shape and motion without depth. *in Proceedings of the Third International Conference in Computer Vision*, pages 91–95, 1990.

[117] P. Torr. Bayesian model estimation and selection for epipolar geometry and generic manifold fitting. *International Journal of Computer Vision*, 50:35–61, 2002.

[118] P. H. S. Torr and D. W. Murray. The development and comparison of robust methods for estimating the fundamental matrix. *International Journal of Computer Vision*, 24:271–300, 1997.

[119] B. Triggs, P. F. McLauchlan, R. Hartley, and A. W. Fitzgibbon. Bundle adjustment a modern synthesis. *Vision Algorithms: Theory and Practice*, 1883:298–372, 2000.

[120] C. Villani. *Topics in optimal transportation*. Number 58. American Mathematical Soc., 2003.

[121] T. Vynnyk, T. Schultheis, T. Fahlbusch, and E. Reithmeier. 3d-measurement with the stereo scanning electron microscope on sub-micrometer structures. *Journal of the European Optical Society-Rapid publications*, 5, 2010.

[122] S. H. Walker and D. B. Duncan. Estimation of the probability of an event as a function of several independent variables. *Biometrika*, 54(1-2):167–179, 1967.

[123] J. S. Warren. *Modern Optical Engineering*. McGraw-Hill, USA, 2007.

[124] A. Whitmore, A. Agarwal, and L. Da Xu. The internet of thingsa survey of topics and trends. *Information Systems Frontiers*, 17(2):261–274, 2015.

[125] C. Wohler. *3D computer vision efficient methods and applications*. Springer, Germany, 2013.

[126] R. Woodham. Photometric method for determining surface orientation from multiple images. *Optical Engineerings*, 19:139–144, 1980.

[127] C. Wu. Towards linear-time incremental structure from motion. *International Conference on 3D Vision (3DV)*, 2013.

[128] G. Yang, Z. Zhu, and F. Zhuo. The application of saas-based cloud computing in the university research and teaching platform. *IEEE International Conference on Intelligence Science and Information Engineering (ISIE)*, 2011.

[129] J. Yu and J. Lin. An architecture for cloud-based consumer support software-as-a-service. *IEEE International Symposium on Computer, Consumer and Control (IS3C)*, 2014.

[130] A. Yuniarti. 3d surface reconstruction of noisy photometric stereo. *University of Western Australia*, 2007.

[131] W. Zhao. A comprehensive study over flip invariant sift. *Technical Report*, 2011.

[132] S. Zhong, J. Wang, L. Yan, L. Kang, and Z. Cao. A real-time embedded architecture for sift. *Journal of Systems Architecture*, 59:16–29, 2013.

[133] T. Zickler, P. N. Belhumeur, and D. J. Kriegman. Helmholtz stereopsis: Exploiting reciprocity for surface reconstruction. *International Journal of Computer Vision*, 49:215–227, 2002.

[134] A. Zolotukhin, I. Safonov, and K. Kryzhanovskii. 3d reconstruction for a scanning electron microscope. *Pattern Recognition and Image Analysis*, 23(1):168–174, 2013.

Appendices

Appendix A: Publications

[**1**] Tafti, Ahmad P., Andrew B. Kirkpatrick, Zahrasadat Alavi, Heather A. Owen, and Zeyun Yu. "*Recent advances in 3D SEM surface reconstruction.*" Micron 78 (2015): 54-66.

[**2**] Tafti, Ahmad P., Andrew B. Kirkpatrick, Jessica D. Holz, Heather A. Owen, and Zeyun Yu. "*3DSEM: A 3D microscopy dataset.*" Data in brief 6 (2016): 112-116.

[**3**] Tafti, Ahmad P., A. B. Kirkpatrick, H. A. Owen, and Z. Yu. "*3D Microscopy Vision Using Multiple View Geometry and Differential Evolutionary Approaches.*" In Advances in Visual Computing, pp. 141-152. Springer International Publishing, 2014.

[**4**] Tafti, Ahmad P., H. Hassannia, A. Borji, and Z. Yu. "*Computer Vision as a Service: Towards an Easy-To-Use Platform for Computer Vision Researchers.*" CVPR 2015: Vision Industry and Entrepreneur Workshop (VIEW 2015).

[**5**] Tafti, Ahmad P., Hamid Hassannia, Dee Piziak, and Zeyun Yu. "*SeLibCV: A Service Library for Computer Vision Researchers.*" In Advances in Visual Computing, pp. 542-553. Springer International Publishing, 2015.

[**6**] Tafti, A. P., Baghaie, A., Kirkpatrick, A. B., Owen, H. A., DSouza, R. M., and Yu, Z. (2016). "*A Comparative study on the application of SIFT, SURF, BRIEF and ORB for 3D surface reconstruction of electron microscopy images.* Computer Methods in Biomechanics and Biomedical Engineering: Imaging & Visualization.

[**7**] Tafti, A. P., Holz, J., Baghaie, A., Owen, H. A., and Yu, Z. (2016). "*3DSEM++: adaptive and intelligent 3D SEM surface reconstruction.* Submitted to Micron. Under Review.

[**8**] Omrani, E., Tafti, A. P., Fathi Firoozabad, M., Dorri Moghadam, A., Rohatgi, P., D'Souza, R., and Yu, Z. (2016). "*Tribological Study in Micro Scale Using 3D SEM Surface Reconstruction.* Submitted to Tribology International. Under Review.

Appendix B: Awards

[**1**] GE Healthcare Honorable Mention Award, UWM Poster Competition 2015.

[**2**] Travel Grant, for 11th International Symposium on Visual Computing (ISVC), Las Vegas, NV, 2015.

[**3**] Travel Grant, for 10th International Symposium on Visual Computing (ISVC), Las Vegas, NV, 2014.

Curriculum Vitae

Ahmad Pahlavan Tafti

Computer Science Department at University of Wisconsin-Milwaukee
Advisor: Professor, Dr. Zeyun Yu

My primary research interests broadly lie in 3D Computer Vision, Machine Learning, Pattern Recognition, Text Mining, and Big Data and their applications in biological and biomedical sciences. GPA: 3.9

Address:
3200 N, Cramer St.
Dept. of Computer Science
University of Wisconsin Milwaukee
Milwaukee, WI 53211, USA.

E-mail:
pahlava2@uwm.edu

Personal Web Page:
http://aptafti.com

Education

- **Master in Computer Science** – Software Engineering, IAU, UAE and Iran: 2011
  Thesis title: "*Digital image forgery detection through statistical data embedding in spatial domain and cellular automata*".
  Advisor: Dr. M.V.Malakooti.
  Co-Advisor: Dr. M. Ashourian.

- **Bachelor in Computer Science** – Software Engineering, IAU, Iran: 1998
  Thesis title: "*Simulation of Basic Computer Architecture*".
  Advisor: Dr. M.H.Yaghmayii.

- **Coursera: Practical Machine Learning,** John Hopkins University: 2016.

- **Coursera: R Programming,** John Hopkins University: 2015.

- **International Studies: Summer School on Image Processing (SSIP 2012); Medical Image Analysis, Visualization and Retrieval**- at Technical University of Vienna and Medical University of Vienna, Vienna, Austria: 2012

- **International Studies: Enterprise Oracle DBA Part 1A**, Architecture and Administration- at ORACLE Education Center, KL, Malaysia: 2001

- **International Studies: Enterprise Oracle DBA Part 1B**, Backup and Recovery Workshop- at ORACLE Education Center, KL, Malaysia: 2001

- **International Studies: Enterprise Oracle DBA Part 2**, Performance Tuning- at ORACLE Education Center, KL, Malaysia: 2001

Fields of Interests

3D Computer Vision, Machine Learning, Pattern Recognition, Text Mining, and Big Data.

Professional and Work Experiences

- **Marshfield Clinic Research Foundation, WI, Marshfield, USA.**   Summer 2015
  Graduate Research Assistant Intern [Link]

  Graduate Research Assistant Intern for the following project:
  - Data Mining Biomedical Literature in the Cloud

  Using Machine Learning strategies, Natural Language Processing techniques, and Big Data infrastructures, such as Apache Hadoop cluster, Apache Spark components, and a Cassandra Database, we designed and developed a scalable framework for large scale biomedical text mining in cancer research.
  I presented my summer project at MCRF Research Symposium 2015. My presentation starts at the time slot **00:54:00** there.

- **University of Wisconsin Milwaukee, WI, Milwaukee, USA.**   Since Jan.2013
  Biomedical Modeling and Visualization Lab.
  Graduate Research Assistant & Developer [Link]

- **University of Wisconsin Milwaukee, WI, Milwaukee, USA.**   Since Jan.2013
  Graduate Teaching Assistant [Link]

  Graduate Teaching Assistant for the following courses:
  - Introduction to Engineering Programming in Matlab (CS 240)
  - Introductory Computer Programming in Java (CS 250)
  - Introduction to Software Engineering (CS 361)
  - Introduction to Database Systems (CS 557)
  - Capstone Project (CS 595)

- **ASYCUDA Project (IRICA), Mashhad, Iran.**   1998-2012
  Database Administrator

Editorial Board and Technical Reviewer Activities

- **International Journal of Rough Sets and Data Analysis, USA.**   Since Feb. 2016
  Technical Reviewer [Link]

- **Verizona Publisher, UK.**   Since Nov. 2015
  Editorial Board Member [Link]

- **International Journal of Computer Vision & Signal Processing, Bangladesh.**   Since Oct. 2015
  Editorial Board Member [Link]
- **International Journal of Computer Vision and Image Processing, USA.**   Since Oct. 2015
  Technical Reviewer [Link]

- **Science Publishing Group, USA.**   Since Aug. 2014
  Editorial Board Member [Link]
  Technical Reviewer [Link]

- **Scientific Online, USA.**   Since Aug. 2015
  Technical Reviewer [Link]
  Technical Reviewer [Link]

- **IEEE International Conferences**   Since Jan. 2014
  Technical Reviewer [Link]
  Technical Reviewer at IEEE international conferences handled by SDIWC

<div style="background:red;color:white">

Publications (Journal Articles and Conference Papers)

</div>

[1] Tafti, A.P., Ye Z, He KY, Wang K, and He MM, "SparkText: Biomedical Text Mining on Big Data Framework and its Application to Cancer Research". *Under Review*. PLOS ONE.

[2] Tafti, A.P., Kirkpatrick, A.B., Holz, J.D., Owen, H.A. and Yu, Z., 2016. 3DSEM: A 3D microscopy dataset. Data in Brief, 6, pp.112-116.

[3] Tafti, A.P., Hassannia, H., Piziak, D. and Yu, Z., 2015. SeLibCV: A Service Library for Computer Vision Researchers. In Advances in Visual Computing (pp. 542-553). Springer International Publishing.

[4] Tafti, A.P., Baghaie, A., Kirkpatrick, A.B., Holz, J.D., Owen, H.A., D'Souza, R.M. and Yu, Z., 2016. A Comparative study on the application of SIFT, SURF, BRIEF and ORB for 3D surface reconstruction of electron microscopy images. Computer Methods in Biomechanics and Biomedical Engineering: Imaging & Visualization, pp.1-14.

[5] Zhao, M., Luo, H., Tafti, A.P., Lin, Y. and He, G., 2015. A Hybrid Real-Time Visual Tracking Using Compressive RGB-D Features. In Advances in Visual Computing (pp. 561-573). Springer International Publishing.

[6] Tafti, A.P., Kirkpatrick, A.B., Alavi, Z., Owen, H.A. and Yu, Z., 2015. Recent advances in 3D SEM surface reconstruction. Micron, 78, pp.54-66.

[7] Tafti, A.P., Hassannia, H., Borji, A., and Yu, Z., 2015. Computer Vision as a Service: Towards an Easy-To-Use Platform for Computer Vision Researchers. CVPR 2015: Vision Industry and Entrepreneur Workshop (VIEW 2015).

[8] Tafti, A.P., Hassannia, H. and Yu, Z., 2015. siftservice. com-Turning a Computer Vision algorithm into a World Wide Web Service. arXiv preprint arXiv:1504.02840.

[9] Tafti, A.P., Kirkpatrick, A.B., Owen, H.A. and Yu, Z., 2014. 3D microscopy vision using multiple view geometry and differential evolutionary approaches. In Advances in Visual Computing (pp. 141-152). Springer International Publishing.

[10] Tafti, A.P. and Maarefdoust, R., 2013. Digital Images Encryption in Spatial Domain Based on Singular Value Decomposition and Cellular Automata. International Journal of Computer Science and Information Security, 11(4), p.121.

[11] Malakooti, M.V., Tafti, A.P. and Naji, H.R., 2012, May. An efficient algorithm for human cell detection in electron microscope images based on cluster analysis and vector quantization techniques. In Digital Information and Communication Technology and it's Applications (DICTAP), 2012 Second International Conference on (pp. 125-129). IEEE.

[12] Tafti, A.P., Malakooti, M.V., Ashourian, M. and Janosepah, S., 2011, August. Digital image forgery detection through data embedding in spatial domain and cellular automata. In Digital Content, Multimedia Technology and its Applications (IDCTA), 2011 7th International Conference on (pp. 11-15). IEEE.

[13] Tafti, A.P. and Janosepah, S., 2011. Digital images encryption in frequency domain based on DCT and one dimensional cellular automata. In Informatics Engineering and Information Science (pp. 421-427). Springer Berlin Heidelberg.

[14] Tafti, A.P., Janosepah, S., Modiri, N., Noudeh, A.M. and Alizadeh, H., 2011. Development of a Framework for Applying ASYCUDA System with N-Tier Application Architecture. In Software Engineering and Computer Systems (pp. 533-541). Springer Berlin Heidelberg.

Book and Book Chapter

[1] A. Pahlavan Tafti, H. Hassannia, "Active Image Forgery Detection Using Cellular Automata", invited book chapter in Cellular Automata in Image Processing and Geometry (Edited by P. Rosin), Pages 127-145, Springer, 2014. (**Book Chapter**)

[2] A. Pahlavan Tafti, Mahdi Assefi, "System Software", Nama Press, Iran, 2011. (**Book – in Persian Language**)

[3] A. Pahlavan Tafti, Mahdi Assefi, "Delphi 7 Programming: A Reference Guide", Naghoos Press, Iran, 2005. (**Book – in Persian Language**)

Awards and Honors

- **Travel Grant**, for 11th International Symposium on Visual Computing (ISVC), Las Vegas, NV, 2015.
- **GE Healthcare Honorable Mention Award**, UWM Poster Competition, USA: 2015.
- **Travel Grant**, for 10th International Symposium on Visual Computing (ISVC), Las Vegas, NV, 2014.

Talks and Communications

- "Data Mining Biomedical Literature in the Cloud", Marshfield Clinic Research Foundation, SSRIP Symposium 2015, USA: August 2015.

- "Biomedical Text Mining and its Applications in Cancer Research", Marshfield Clinic Research Foundation, Journal Club, USA: July 2015.

- "SIFT as a Service: Turning a Computer Vision Algorithm into a World Wide Web Service", UWM Poster Competition 2015, USA: April 2015

- "3D Microscopy Vision Using Multiple View Geometry and Differential Evolutionary Approaches", The 10th International Symposium on Visual Computing (ISVC), Las Vegas, USA: December 2014.

- "3D Surface Reconstruction of Microscopic Objects", Computer Science Department, University of Wisconsin Milwaukee, USA: April 2014

- "Multiple View Geometry and Structure from Motion", Advanced Computer Graphics class, Computer Science Department, University of Wisconsin Milwaukee, USA: April 2014

- "Particle Filter Segmentation", Summer School on Image Processing (SSIP 2012), Vienna, Austria: July 2012

- "Fault Tolerance Databases", 14th Local Conference for IT Experts, International Exhibition, Mashhad, Iran: May 2011

Qualifications

- **Programming Languages:** Java, SQL, PL/SQL, Matlab, R, Python.

- **Java Technologies:** JSP, Servlets, Spring.

- **DBMS:** Oracle, MySQL, Cassandra, MongoDB.

- **Web Application Server:** Apache Tomcat.

- **Software Engineering:** Agile Software Development, RUP.

- **Protocols:** HTTP.

- **Web Technologies:** SOAP, RESTful.

- **Build Tools:** Maven.

- **Big Data Technologies:** Apache Spark, Apache Spark MLlib, Apache Cassandra, Apache Hadoop.

Membership

- **IEEE** (*Institute of Electrical and Electronics Engineers*), USA.

- **ACM** (*Association for Computing Machinery*), USA.

- **MSA** (*Microscopy Society of America*), USA.

Selected Research/Software Projects

- **SparkText: A Big Data Toolset for Large Scale Biomedical Text Mining**

A large number of biomedical research articles are published every day, accumulating rich information, such as genetic variants, genes, phenotypes, diseases, and treatments. Rapid yet

accurate text mining on large-scale scientific literature can discover novel knowledge to better understand human diseases, and to improve the quality of disease diagnosis, prevention, and treatment. In this project, we designed and developed an efficient text mining framework called "**SparkText**" on a Big Data infrastructure, which is composed of Apache Spark data streaming and machine learning algorithms, combined with Apache Cassandra NoSQL database. The "**SparkText**" is designed for mining large-scale scientific articles published on multiple journals. To demonstrate its performance for classifying cancer types, we extracted information (e.g., breast, prostate, and lung cancers) from thousands of articles, and then employed different classification algorithms to build prediction models. Compared to other tools that took more than 10 hours to mine the 27,001 full text articles, "**SparkText**" took about 5 minutes to mine the same dataset. The "**SparkText**" is **publicly** and **freely** available at **http://sparktext.omicspace.org/** for the research community.

Several computational technologies including machine learning, natural language processing, big data infrastructures, and distributed database systems have been unutilized in this contribution.

- **3DSEM: A 3D Microscopy Dataset**

The Scanning Electron Microscope (SEM) as 2D imaging instrument has been widely used in biology and material sciences to determine the surface attributes of microscopic specimens. However the SEM micrographs still remain 2D images. To effectively measure and visualize the surface properties, we need to restore the shape model from the SEM images. Having 3D surfaces from SEM images would provide true anatomic shape of microscopic objects which allow for quantitative measurements and informative visualization of the system being investigated. The 3D Microscopy Dataset includes both 2D images and 3D reconstructed surfaces of different biological samples as well as micro material objects. The dataset is **publicly** and **freely** available at **http://selibcv.org/3dsem** for any academic, research, and educational purposes.

We employed different computational technologies, such as multi view geometry, 3D computer vision, machine learning, and optimization algorithms to develop the dataset.

- **SeLibCV: A High-Available Service Library for Computer Vision Researchers**

Image feature detectors and descriptors have made a big advance in several computer vision applications including object recognition, image registration, remote sensing, panorama stitching, and 3D surface reconstruction. Most of these fundamental algorithms are complicated in code, and their implementations are available for only a few platforms. This operational restriction causes various difficulties to utilize them, and even more, it makes different challenges to establish novel experiments and develop new research ideas. **SeLibCV** is Software as a Service (SaaS) library specializing in local features detection, extraction, and matching algorithms which offers reusable and platform independent components, leading to reproducible research for computer vision researchers worldwide. The present work facilitates Rapid Application Development (RAD), and provides application-to-application interaction by tiny services accessible through the Internet. **SeLibCV** is **publicly** and **freely** available at **http://selibcv.org/** for any academic, educational and research purposes.

We designed and developed **SeLibCV** using several technologies, such as computer vision, machine learning, SOAP web services, and SaaS architecture.

Please refere to my personal website for further information

http://aptafti.com